Theory of double quantum two-dimensional electron spin resonance with application to distance measurements

Sunil Saxena and Jack H. Freed
Baker Laboratory of Chemistry, Cornell University, Ithaca, New York 14853-1301

(Received 24 February 1997; accepted 23 April 1997)

A formulation is presented for calculating double quantum two dimensional electron spin resonance (DQ-2D ESR) spectra in the rigid limit that correspond to recent experimental DQ-2D ESR spectra obtained from a nitroxide biradical. The theory includes the dipolar interaction between the nitroxide moieties as well as the fully asymmetric g and hyperfine tensors and the angular geometry of the biradical. The effects of arbitrary pulses (strong but not truly nonselective pulses) are included by adapting the recently introduced split Hamiltonian theory for numerical simulations. It is shown how arbitrary pulses in magnetic resonance create ''forbidden'' coherence pathways, and their role in DQ-2D ESR is delineated. The high sensitivity of these DQ-2D ESR signals to the strength of the dipolar interaction is demonstrated and rationalized in terms of the orientational selectivity of the ''forbidden'' pathways. It is further shown that this selectivity also provides constraints on the structural geometry (i.e., the orientations of the nitroxide moieties) of the biradicals. The theory is applied to the recent double quantum modulation (DQM) experiment on an end-labeled poly-proline peptide biradical. A distance of 18.5 Å between the ends is found for this biradical. A new two pulse double quantum experiment is proposed (by analogy to recent NMR experiments), and its feasibility for the ESR case is theoretically explored.
[S0021-9606(97)00729-0]

I. INTRODUCTION

Recently double quantum two dimensional electron spin resonance (DQ-2D ESR) experiments were obtained,[1] on a poly-peptide system, spin labeled with a nitroxide at both ends. This required a novel application of pulses of arbitrary strengths to produce the double quantum coherence. A double quantum electron spin echo (ESE) signal was also reported on spin-correlated radical pairs,[2] wherein the double quantum coherence is ''naturally produced'' by the bond cleavage. Such experiments have opened up a powerful new tool for structural and relaxation studies.

For example, a particularly important application for ESR is the measurement of large distances in doubly labeled macromolecules or between paramagnetic sites in a solid. Such measurements in ESR have thus far largely relied on a large exchange or dipolar coupling leading to an observable difference in the continuous wave spectrum.[3–5] Hence they have been restricted to measurements of less than ca. 15 Å. One approach, might be to measure the homogeneous linewidths (i.e., T_2) in a biradical and extract the distance information from that by comparison with the T_2 from a structurally and chemically similar monoradical used as a standard. However, the extraction of homogeneous linewidths from an inhomogeneously broadened spectrum is often very ambiguous in continuous wave (CW) ESR. The natural candidate for this approach would then be a spin-echo or a SECSY experiment. In the latter case inhomogeneities are refocused in t_1, and hence one obtains the homogeneous linewidths along ω_1.[6] However, the contributions to the homogeneous linewidths in the biradical spectrum due to fluctuations in the intramolecular dipolar interaction, when compared to the monoradical, would fall off rapidly with separation as $(1/r^6)$, where r is the interelectron distance. Hence this method is not expected to be very reliable for larger distances. It would also require an additional experiment that relies on the availability of a suitable monoradical, for the determination of small differences in the T_2's between mono and biradicals and the estimation of a rotational correlation time. In a similar spirit one could measure the difference in T_1 but the nonsecular spectral densities available are typically small.[7]

The advantage of double quantum ESR is that one can, with appropriate phase cycling, isolate the double quantum signal which carries the dipolar information directly in its modulation pattern.[1] Since this coherence depends on the dipolar interaction, the intensity of this signal falls off more slowly ($\sim 1/r^3$) and therein lies the possibility for measuring larger distances. Also, the calibration using a monoradical is not required.

Single quantum selective pulse methods have been developed for measuring distances, based on double electron–electron resonance[8,9] (DEER) and on the ''$2+1$'' pulse train.[10,11] The success of these methods in measuring distances greater than 15 Å, is encouraging. In particular, Larsen and Singel[9] were able to measure the dipolar coupling directly from the spectrum, after appropriate signal processing. However, the advantage of the double quantum coherence method is that the measured signal is directly due to the dipolar interaction (by the very nature of generation of DQ coherences), and hence it has a greater sensitivity towards this interaction. For this reason the analysis of a DQ coherence experiment to extract distances is cleaner than the other methods.[1] For example, in the DEER based technique[9] the weak dipolar echo modulation has to be extracted from the

dominant background echo decay by spectral subtraction (assuming a simple exponential decays for the background signal). In addition, the DQ signal is unaffected by monoradical impurities, while the other techniques may have to correct for these signals. Another important advantage would be that, in the DQ method we can measure the double quantum relaxation rate (T_2^D) directly. This has the potential of significantly aiding the elucidation of motional dynamics[1] (cf. below).

The use of double spin labeling of macromolecules for distance measurements is analogous to the method of fluorescence energy transfer (FET). However, distances measured from FET suffer from large uncertainties in the κ^2 parameter that describes the relative orientation of the transition dipoles of the two chromophores.[12] No comparable problem exists in ESR, since the spins are quantized along the magnetic field.

As mentioned above, another important application of double quantum ESR would be the elucidation of motional dynamics in conjunction with (and in analogy to) single quantum methods like COSY/SECSY and 2D ELDOR.[6,13] For example, a simple comparison of the double and single quantum linewidths (i.e., T_2's) would provide a clue for correlated vs uncorrelated dynamics,[1] (i.e., overall rotation as opposed to local motions). This would be of significant relevance for studies on flexible biomolecules, like proteins.

In this paper, we present a detailed analysis of such DQ experiments, with the aim of improving the sensitivity, resolution, and range of the DQ technique that we have developed.[1] Also, other approaches for measuring the DQ signal are discussed. To this end, we consider the full complexity of the nitroxide Hamiltonian. Therefore, we include the completely anisotropic g and hyperfine tensors and the angular geometries of the biradical (cf. Fig. 1).

Further, we treat the effect of the finite pulses in detail. The key feature of these DQ experiments[1] was the creation of a double quantum coherence by an arbitrary pulse (i.e., a strong but not completely nonselective pulse: $\epsilon \sim H$, where ϵ represents the effect of a pulse and H the internal Hamiltonian of the system). The effects of the arbitrary pulse are therefore considered in detail. In general, such cases in magnetic resonance are dealt with by ''brute force'' diagonalization,[14] which lacks the predictive power that an analytic theory provides. Recently, a number of analytic methods[15] have been proposed to deal with the case of weak (i.e., $\epsilon < H$) and/or selective pulses for other applications (mainly for nuclear modulation in ESR). These are, of course, not immediately applicable for our case because our pulses are neither weak nor truly selective. However, recently a new theoretical method called split Hamiltonian theory (SHT) has been developed to deal with the case of arbitrary pulses in magnetic resonance.[16] We have used SHT to account for the role of the pulses in our experiments (cf. Sec. II B). Not only does this method provide accurate numerical results, but in lowest order, tractable analytical expressions may be readily obtained, that while not necessarily quantitative, do describe the formation and general properties (such as orientational selectivity, cf. below) of the DQ coherences that are created by finite pulses in magnetic resonance (cf. Sec. IV). The insight provided by the use of SHT has lead us to an alternative approach for the creation of DQ coherences that is useful for the measurement of distances (cf. Sec. III B).

In this paper, we first consider the single quantum (SQ) COSY/SECSY signal from a biradical. We then show how the same two pulse sequence may be used to detect DQ signals, by analogy with recent NMR observations.[14,17,18] The feasibility of such experiments for ESR is theoretically explored. We then consider the DQ ESR experiments that have already been experimentally performed.[1] These are five pulse experiments which are based on the creation of extra DQ coherences due to the arbitrary pulses.[1] The first case is the double quantum modulation (DQM) experiment. In the time domain this provides a simple method of measuring the dipolar interaction. The second is the DQ-COSY experiment, which provides information on the DQ relaxation rate (i.e., T_2^D). Next, we turn to the detection of the primary DQ echo based on a six pulse sequence. Finally, we compare the DQM experiment to theory.

This work validates the key observations of our first communication.[1] The DQ signals we see are additional and/or ''forbidden'' coherences created by the second and third pulses of the five pulse sequence. The forbidden nature of these signals also provides an orientational selectivity, such that the signal primarily arises from those orientations of the dipolar vector that are parallel (or nearly so) to the dc magnetic field. It is this orientational selectivity that causes the signal to be very sensitive to the dipolar interaction, and hence to the interelectron distance. We further show that this orientational selectivity leads to a structural sensitivity, i.e., the signals are sensitive to the orientations of the two nitroxides. This has significant potential for structural studies in biomolecules. Also, we demonstrate from theoretical simulations, that the primary or ''allowed'' echo arising from a basic six pulse sequence, (which lacks this orientational selectivity), has a much reduced intensity compared to the ''forbidden'' DQM/DQ-COSY echoes. This is undoubtedly the reason why we were unable to observe the primary echo.[1]

The appropriate theory for these experiments is summarized in Sec. II, with more detailed descriptions of the derivations given in the Appendices. The two pulse single and double quantum experiments are discussed in Sec. III. The case of the five pulse DQM/DQCOSY is presented in Sec. IV, and the six pulse primary DQ signal in Sec. V. The theory is compared to experiment in Sec. VI, and the conclusions are given in Sec. VII.

II. THEORY

In this section we provide the theory for calculating double quantum 2D ESR spectra for nitroxide biradicals. The underlying model consists of a rigid biradical with well defined orientations of the two nitroxides with respect to the dipolar vector. This is illustrated in Fig. 1(a) and relevant coordinate frames are shown in Fig. 1(b). In Sec. II A we give the spin Hamiltonian for this rigid system, with more

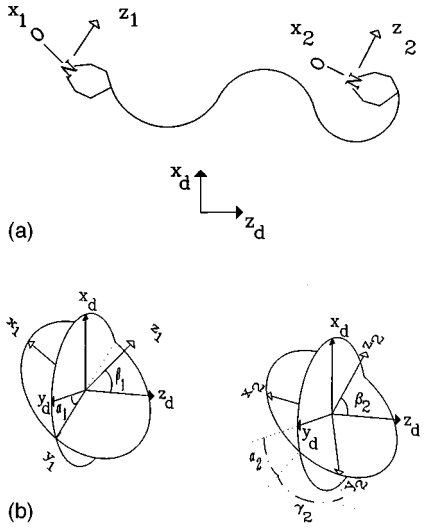

FIG. 1. (a) A schematic drawing of a biradical defining the convention used for the axis systems of the magnetic g and hf tensors: The z axes are along the $N\pi$ orbitals and the x axes are along the N–O bond. The y axes are in the plane of the ring. (b) The relevant Euler angles required to transform from the dipolar to the molecular frame. These Euler angles define the angular geometry of the molecule.

details provided in Appendix A. In Sec. II B we describe how the signal is calculated, and we show how SHT is adapted for the numerical calculations.

A. Spin Hamiltonian

In order to deal properly with the 2D ESR spectra we include the fully asymmetric g and hyperfine (hf) tensors. In that case, the internal Hamiltonian for a nitroxide biradical is given by

$$H=H_1+H_2+H_D+H_J, \tag{1}$$

where H_i $(i=1,2)$ is the contribution from the hyperfine and Zeeman terms of the two nitroxides and H_D and H_J are the contributions from the dipolar and (isotropic) exchange interactions, respectively. The terms H_i $(i=1,2)$ can be written as

$$H_i=C_iS_{z_i}+A_iS_{z_i}I_{z_i}+B_iS_{z_i}I_{+1_i}+B^*S_{z_i}I_{-1_i} \tag{2}$$

when as is usual, the hf terms nonsecular in $\mathbf{S_i}$ are neglected, (i.e., the high field approximation). Explicit expressions for the terms C_i, A_i, and B_i are provided in Appendix A. They contain the anisotropies in the g and hf tensors and are dependent on the Euler angles $(\alpha_i,\beta_i,\gamma_i)$ that describe the orientation of the respective g and hf tensors relative to the dipolar frame, and also the angles (θ,ζ) that define the orientation of the interspin dipolar frame relative to the dc magnetic field. Note that we assume the respective g and hf tensors of each nitroxide to have the same principal axis systems (PAS). This is clarified in Fig. 1 where we show the PAS's of the two nitroxides and the Euler angles required to transform the g and A tensors to the lab frame.

We assume axial symmetry of the dipolar interaction, which is appropriate for the case of interest to us, of biradicals wherein the electron spins are well separated. This term can then be written as[19]

$$H_D=\frac{D}{2}\,(3\cos^2\,\theta-1)[S_z^2-\tfrac{1}{3}\mathbf{S}^2], \tag{3}$$

where

$$S_z=S_{z_1}+S_{z_2}, \tag{4}$$

$$\mathbf{S}=\mathbf{S_1}+\mathbf{S_2}, \tag{5}$$

and D is the dipolar spin–spin interaction parameter, which we shall express in Gauss (G). For a given interelectron distance, r (in Angstroms), this parameter D (in G) is given by[5]

$$D=\frac{3g\beta_e}{2r^3}, \tag{6}$$

where g is the isotropic g value and β_e is the value of the Bohr magneton.

The spin exchange term is taken to be[20]

$$H_J=J(\tfrac{1}{2}-2\mathbf{S_1}\cdot\mathbf{S_2}), \tag{7}$$

where J is the strength of the exchange interaction.

Finally, during a pulse of duration t_p, the Hamiltonian is

$$H_p=H+\epsilon \tag{8}$$

with H given by Eq. (1). The effect of the radiation field during pulses is given by ϵ, with

$$\epsilon(t_p)=\frac{\omega_1}{2}\,(\epsilon^{-i\phi}S_+ + e^{i\phi}S_-), \tag{9}$$

where ϵ is the irradiating microwave pulse of duration t_p, intensity, B_1 $(=\omega_1/\gamma_e$ with γ_e the gyromagnetic ratio for the electron spin), and phase ϕ. Also

$$\begin{aligned} S_+&=S_{1+}+S_{2+}\,,\\ S_-&=S_{1-}+S_{2-}\,. \end{aligned} \tag{10}$$

The nominal flip angle of the pulse is defined as β. This is given by

$$\beta=\omega_1 t_p\,. \tag{11}$$

Equations (1), (2), (3), (7), and (9) then define the Hamiltonian we use for the case of nitroxide biradicals.

B. Calculation of the ESR signal

To calculate the ESR signal, one first describes the time evolution of the spin density matrix, ρ, by the equation[21–23]

$$\frac{d}{dt}\,\rho=-i[H(t),\rho(t)]-\hat{\hat{\Gamma}}(\rho(t)-\rho_0). \tag{12}$$

In Eq. (12), H is given by Eq. (1) in the absence of radiation and $\rho(0)=\rho_0\propto S_z$, where ρ_0 is the equilibrium spin density matrix. Also, $\hat{\hat{\Gamma}}$ is the relaxation superoperator. Denoting the

difference between the time dependent density matrix, $\rho(t)$, and the equilibrium density matrix, ρ_0 by χ we get

$$\frac{d}{dt}\chi = -i[H(t),\chi(t)] - \hat{\hat{\Gamma}}\chi(t) \equiv \hat{\hat{\Gamma}}'\chi(t). \tag{13}$$

Relaxation will be treated phenomenologically, with orientation independent relaxation rates T_1, T_2^S, and T_2^D, where the superscripts S and D refer to single and double quantum relaxation times, respectively. Then the superoperator $\hat{\hat{\Gamma}}'$ in the eigenbasis of the spin Hamiltonian, H of Eq. (1) (cf. Appendix B), is given by[24]

$$\hat{\hat{\Gamma}}'_{ij,kl} = \delta_{ik}\delta_{jl}\left[-i\omega_{ij} - \delta_{ij}\frac{1}{T_1} - \left(1-\delta_{ij}\frac{1}{T_2^K}\right], \quad K=S,D, \right. \tag{14}$$

$$\omega_{ij} = E_i - E_j, \tag{15}$$

where ω_{ij} are the resonant frequencies, given as the differences of eigenenergies E_i, in the rotating frame. These eigenenergies are derived in Appendix B and are obtained from Eq. (B13). Equation (13) is then solved in the form[24]

$$\chi(t_0+t)_{ij} = e^{\hat{\Gamma}'_{ijij}t}\chi(t_0)_{ij}, \tag{16}$$

where the χ_{ij} are expressed in the eigenstates of Eqs. (B5) and (B11). In Appendix B we also provide the matrix representation for the spin Hamiltonian given by Eq. (1), and also explicit expressions for e^{-iHt}.

During a pulse, spin relaxation will be neglected, so the density matrix will evolve as

$$\frac{d}{dt}\rho = -i[(H+\epsilon),\rho(t)]. \tag{17}$$

The formal solution to Eq. (17), after a pulse of duration, t_p, is given by

$$\rho(t_0+t_p) = \epsilon^{-i(H+\epsilon)t_p}\rho(t_0)e^{i(H+\epsilon)t_p}. \tag{18}$$

In the usual nonselective pulse approximation, ϵ is deemed to be much greater than H (i.e., $\epsilon \gg H$) during t_p, and hence one needs to calculate only $e^{-i\epsilon t_p}$. However, in 2D ESR (and in solid state NMR) the pulses are typically not truly nonselective. We shall instead refer to them as *arbitrary*. In fact, the finiteness of ϵ is crucial for generating a class of double (and in general multiple) quantum coherences.[1,14,17,18] The inability of an arbitrary pulse to uniformly excite the magnetic resonance spectrum leads to significant off-resonance effects, like a frequency dependent variation in phase and intensity.[22,25] More subtly, arbitrary pulses also create extra coherence pathways, which lead to ''ghost'' and ''phantom'' echoes in 2D NMR spectroscopy.[26] These effects were considered to be artifacts and phase cycling sequences were devised to eliminate them.[26(a)] However, there has been a rejuvenated interest in characterizing[27–29] and utilizing these large effects.[1,14,17,18]

Hence one needs to calculate $e^{-i(H+\epsilon)t_p}$ explicitly. The usual approach has been to numerically diagonalize $e^{-i(H+\epsilon)t_p}$.[14] While this approach is useful for quantitative analysis, it lacks the predictive power of an analytic theory.

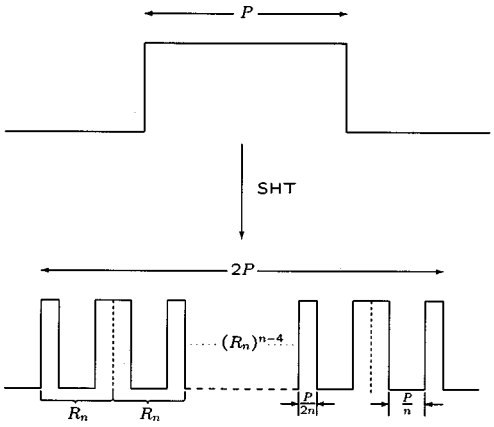

FIG. 2. The nth order split Hamiltonian theory approximation for an arbitrary pulse of duration P.

To this end a new theoretical method, called split Hamiltonian theory (SHT)[16] has been proposed recently, to deal with this situation of arbitrary pulses in magnetic resonance. Here, an arbitrary pulse is reconstructed as a series of $2n$ nonselective pulses of duration $(t_p/2n)$ each, interspersed with periods of free evolution of duration (t_p/n). Figure 2 shows the decomposition of an arbitrary pulse into the nth degree SHT approximation. In this example each subpulse sequence is composed of a nonselective pulse of duration $P/2n$ followed by a period of free evolution of duration P/n and another nonselective pulse of duration $P/2n$. The mathematical validity for this approach is based on the symmetrized Suzuki–Trotter formula,[30,31] which can be written in this context as

$$R \equiv e^{-i(H+\epsilon)t_p} = \lim_{n\to\infty}(e^{-i\epsilon t_p/2n}e^{-iHt_p/n}e^{-i\epsilon t_p/2n})^n. \tag{19}$$

Defining

$$R_n = e^{-i\epsilon t_p/2n}e^{-iHt_p/n}e^{-i\epsilon t_p/2n}, \tag{20}$$

we have

$$R = \lim_{n\to\infty}(R_n)^n. \tag{21}$$

Each exponential on the right-hand side of Eq. (19) can usually be written explicitly in an appropriate basis and hence analytic expressions for R can be determined for a desired value of the exponent, n. Further, Salikhov *et al.*[16] demonstrated that values of 2–4 of the Trotter exponent, n, for a model Hamiltonian were sufficient to provide satisfactory approximations to $e^{-i(H+\epsilon)t_p}$ when compared to the exact results. The advantage of SHT, then, is that it provides analytic formulas for the signal which can also be numerically iterated for more quantitative calculations, if required. For example, even the lowest order of Eq. (19) (i.e., $n=1$) conveys the essential physics of the problem like the generation of extra coherences (cf. Sec. IV, below). We have used this approach to deal with the pulses in the experiments considered and a value of 8 for n was found to be sufficient for numerical convergence for the estimated value of $B_1 = 17.8$ G currently available in our spectrometer. For the

case of weak pulses of strength ($B_1=1.8$ G) used for some simulations, $n=16$ was used. The expressions for $e^{-i\epsilon t_p}$ required in Eq. (19) are provided in Appendix C.

Note that in Eq. (19) we have defined R_n in a form that is a variant of that used by Salikhov *et al.* That is they used the choice[16]

$$R_n = e^{-iHt_p/2n} e^{-i\epsilon t_p/n} e^{-iHt_p/2n}. \tag{22}$$

While these choices are arbitrary in the formulation of SHT, the convention of Salikhov *et al.* [Eq. (22)] results in more tractable analytical calculations for a given value of n, since the periods of free evolution that occur in the extremities of R can be combined with the time intervals just preceding and just following the pulse. However, note that in our convention the $n=1$ approximation already breaks up the arbitrary pulse into two subpulses, whereas, this requires the $n=2$ approximation in the convention of Salikhov *et al.* In this sense their n subpulse approximation is related to the $n-1$ subpulse approximation in our convention. The value of the present approach is that the effects of an arbitrary pulse can be discussed at a lower order of n. Using Eq. (19), $R \equiv e^{-i(H+\epsilon)t_p}$ can be shown to have the form

$$R = \begin{pmatrix} R_{11} & R_{12}e^{-i\phi} & R_{13}e^{-i\phi} & R_{14}e^{-2i\phi} \\ R_{21}e^{i\phi} & R_{22} & R_{23} & R_{24}e^{-\phi} \\ R_{31}e^{i\phi} & R_{32} & R_{33} & R_{34}e^{-i\phi} \\ R_{41}e^{2i\phi} & R_{42}e^{i\phi} & R_{43}e^{i\phi} & R_{44} \end{pmatrix}, \tag{23}$$

where the elements R_{ij}, are independent of the phase ϕ of the pulse.

This characteristic labeling in ϕ means that each coherence pathway is distinctly defined by the phase of each pulse, and hence efficient phase cycling sequences can be easily determined to experimentally select desired coherence pathways. Also, this allows us to selectively calculate the signal from a given coherence pathway. Note that the R_{ij} are dependent on the strength, B_1 and duration, t_p of the pulse, and also on the resonant frequencies, ω_{ij}.

For the sake of convenience of notation, the propagation operator $e^{i(H+\epsilon)t_p}$ can be similarly written down as a matrix P. From the unitary property of the operator $e^{i(H+\epsilon)t_p}$

$$P_{ij} = R^*_{ji}. \tag{24}$$

We choose the dipolar frame as the main symmetry axis of the molecule. The signal, $F_+(t)$, is calculated for each orientation of the dipolar vector with respect to the dc magnetic field (given by the angles θ and ζ) as

$$F_+(t,\theta,\zeta) = \mathrm{Tr}[S_+\rho(t)]. \tag{25}$$

Using Eqs. (16) and (18) we can obtain $\rho(t)$ for the relevant coherence pathway(s) from a sequence of pulses, and then the signal, F due to each orientation [cf. Eq. (25)] can be written as a combination of terms dependent on the pulse (i.e., $R_{ij}=P^*_{ji}$) and on the resonant frequencies (i.e., ω_{ij}). Combinations of the terms in ω_{ij}, which appear in the signal, are given in Table I. These are denoted by S^i_j (the subscript labels the different terms, while the superscript, i, is

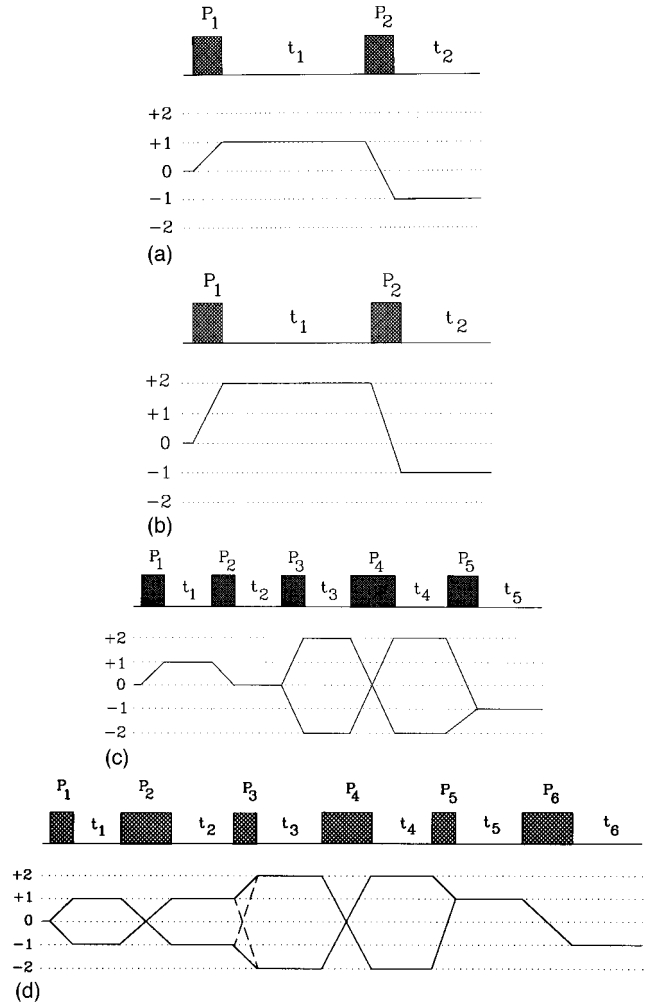

FIG. 3. Pulse sequence used. (a) Two pulse COSY/SECSY sequence. (b) Two pulse DQ sequence. (c) Five pulse sequence used for DQM/DQ-COSY experiments. (d) Six pulse sequence used for a refocused DQ echo experiment. Relevant coherence pathways are also shown.

TABLE I. Terms defining the signal due to each orientation. Note that the superscript, i, is used to label the time interval while the subscripts labels each term. $\omega_{ij}=E_i-E_j$. The E_i, $i=1,2,3$, or 4 are given by Eq. (B13), and Φ is given by Eq. (B10).

S^i_1	$\cos^2\Phi e^{-i\omega_{12}t_i}+\sin^2\Phi e^{-i\omega_{13}t_i}$
S^i_2	$\cos\Phi\sin\Phi\{e^{-i\omega_{12}t_i}-e^{-i\omega_{13}t_i}\}$
S^i_3	$\cos^2\Phi e^{-i\omega_{24}t_i}+\sin^2\Phi e^{-i\omega_{34}t_i}$
S^i_4	$\cos\Phi\sin\Phi\{e^{-i\omega_{24}t_i}-e^{-i\omega_{34}t_i}\}$
S^i_5	$\sin^2\Phi e^{-i\omega_{12}t_i}+\cos^2\Phi e^{-i\omega_{13}t_i}$
S^i_6	$\sin^2\Phi e^{-i\omega_{24}t_i}+\cos^2\Phi e^{-i\omega_{34}t_i}$

TABLE II. Phase cycling for two pulse double quantum experiment. This two step cycle is augmented by the addition of CYCLOPS making it an eight pulse sequence.

P_1	P_2	Sign
0	0	+
180	0	+

used to label the relevant time intervals). The powder pattern is calculated by integrating over all the orientations of the dipolar vector

$$S(t)=\int_0^{2\pi} d\zeta \int_0^{\pi} \sin\,\theta F_+(t,\theta,\zeta)\,d\theta. \tag{26}$$

Using Eqs. (16), (18), (19), and (24), the signal from any pulse sequence can be calculated. Signals from the pulse sequence and coherence pathways shown in Fig. 3 were calculated in this manner. These are discussed in the next three sections. The phase cycling for the two pulse and five pulse DQ experiments is provided in Tables II and III, respectively.

III. TWO PULSE EXPERIMENTS

We begin with the simplest of two dimensional experiments, i.e., two pulse experiments. In Sec. III A single quantum COSY and SECSY experiments are discussed. Recently, double quantum 2D NMR experiments using the two pulse sequence have been performed.[14,17,18] In Sec. III B we discuss the feasibility of such experiments for the 2D ESR case.

TABLE III. Phase cycling for five pulse double quantum experiment. This four step cycle is augmented by the additional four steps in parentheses, to which CYCLOPS is then added.

P_1	P_2	P_3	P_4	P_5	Sign
0 (180)	0 (0)	0 (0)	0 (0)	0 (0)	+ (−)
90 (270)	90 (90)	90 (90)	0 (0)	0 (0)	− (+)
180 (0)	180 (180)	180 (180)	0 (0)	0 (0)	+ (−)
270 (90)	270 (270)	270 (270)	0 (0)	0 (0)	− (+)

A. Single quantum signals: COSY and SECSY experiments

In the single quantum COSY experiment the first pulse creates transverse magnetization (± 1 coherences). The signal is measured after the second pulse. Formally, the SECSY signal is related to the COSY signal by the transformation $t_2 \rightarrow t_2 + t_1$.[22,32] In the SECSY experiment the inhomogeneities are refocused in t_1 and hence this experiment provides the homogeneous single quantum linewidths along ω_1.[6] The COSY S_{C-}[24,32] signal (given by the coherence pathway $0 \underset{\pi/2}{\longrightarrow} +1 \underset{\pi/2}{\longrightarrow} -1$) for each orientation of the dipolar vector can be written as

$$\begin{aligned} F^{\mathrm{COSY}}(t_1,t_2)=e^{2i\phi^2}e^{-i\phi^1}[&S_3^{2*}R_{42}^2P_{42}^2\{S_3^1(R_{21}^1P_{14}^1-R_{24}^1P_{44}^1)+S_4^1(R_{31}^1P_{14}^1-R_{34}^1P_{44}^1)\}\\ &+S_4^{2*}R_{43}^2P_{43}^2\{S_4^1(R_{21}^1P_{14}^1-R_{24}^1P_{44}^1)+S_3^1(R_{31}^1P_{14}^1-R_{34}^1P_{44}^1)\}+S_1^{2*}R_{21}^2P_{21}^2\{S_1^1(R_{11}^1P_{12}^1-R_{14}^1P_{42}^1)\\ &+S_2^1(R_{11}^1P_{13}^1-R_{14}^1P_{43}^1)\}+S_2^{2*}R_{31}^2P_{31}^2\{S_2^1(R_{11}^1P_{12}^1-R_{14}^1P_{42}^1)+S_1^1(R_{11}^1P_{13}^1-R_{14}^1P_{43}^1)\}]\\ &\times e^{-(t_1+t_2)/T_2^S}e^{-2\pi^2\Delta_G^2(t_2-t_1)^2}. \end{aligned} \tag{27}$$

The terms R and P in Eq. (27) are given by Eqs. (19) and (24), respectively, while the terms, S, are given in Table I. The superscripts on R, P, and ϕ are used to label the pulses (cf. Fig. 3) to which these terms refer (they are *not* exponents). Δ_G represents sources of inhomogeneous broadening, which are refocused in a spin–echo,[32–34] and are assumed to be Gaussian.

While the dominant interactions are the hf interactions, fluctuations in the dipolar interaction would lead to a smaller homogeneous T_2^S for the biradical as compared to the monoradical in the COSY experiment. This is treated only phenomenologically in these simulations.

The efficiency of single quantum coherence transfer, (i.e., the extent of the transfer $0 \rightarrow 1$), $T_{0\rightarrow 1}$, due to the first pulse is given by

$$\begin{aligned} T_{0\rightarrow 1}=2\times[&(R_{21}^1P_{14}^1-R_{24}^1P_{44}^1)+(R_{31}^1P_{14}^1-R_{34}^1P_{44}^1)\\ &+(R_{11}^1P_{12}^1-R_{14}^1P_{42}^1)+(R_{11}^1P_{13}^1-R_{14}^1P_{43}^1)]. \end{aligned} \tag{28}$$

Also the efficiency of back coherence transfer due to the second pulse, $T_{1\rightarrow -1}$ is given by

$$T_{1\rightarrow -1}=R_{42}^2P_{42}^2+R_{43}^2P_{43}^2+R_{21}^2P_{21}^2+R_{31}^2P_{31}^2. \tag{29}$$

The primary value of Eqs. (27), (28), and (29) is that they allowed us to meaningfully evaluate the intensities of the double quantum signals and transfer efficiencies discussed in Secs. III B, IV, and V.

B. Double quantum signal

We would now like to deal with the generation of an extra (multiple quantum) coherence with a single pulse and its detection with a second pulse. This idea was demonstrated very early in NMR[35,36] as ''forbidden transitions'' and put in the modern magnetic resonance terminology of multiple quantum transitions by several workers.[27–29] Recently there has been a resurgence of interest in experimentally exploiting this feature in NMR.[14,17,18] The first pulse in this sequence creates a double (or multiple) quantum coherence, which then evolves for a period t_1. A second pulse transfers this double (multiple) quantum coherence into observable single quantum coherence. The signal is measured after the second pulse for a series of values of t_1. The phase cycling for this two pulse DQ sequence is provided in Table II.

This double quantum signal from a two pulse sequence, is given by the coherence pathway

$0 \xrightarrow{\pi/2} +2 \xrightarrow{\pi/2} -1$. The first pulse creates an extra coherence, i.e., 2. This is given by $(R^1_{11}P^1_{14}-R^1_{14}P^1_{44})$, where R and P are defined in Eqs. (19) and (24), respectively. For a nonselective pulse [cf. Eq. (C7) in Appendix C]

$$R_{11}=\tfrac{1}{2}(\cos\beta+1),$$
$$P_{14}=\tfrac{1}{2}(\cos\beta-1),$$
$$R_{14}=\tfrac{1}{2}(\cos\beta-1), \tag{30}$$
$$P_{44}=\tfrac{1}{2}(\cos\beta+1).$$

Hence $(R^1_{11}P^1_{14}-R^1_{14}P^1_{44})$ is zero. However, for arbitrary pulses this term is nonzero. For example in the lowest order $(n=1)$ SHT approximation of Eq. (19) [obtained using Eqs. (B15) and (C7) and representing R and P in the singlet–triplet representation] this coherence transfer is given by

$$\begin{aligned}T_{0\to 2}\equiv R_{11}P_{14}-R_{14}P_{44}=e^{-2i\phi^1}\Bigg\{&\left[\frac{1}{4}\left(\cos\left(\frac{\beta}{2}\right)+1\right)^2 e^{-iE_1t_p}+\frac{1}{4}\left(\cos\left(\frac{\beta}{2}\right)-1\right)^2 e^{-iE_4t_p}-\frac{1}{2}\sin^2\left(\frac{\beta}{2}\right)\left(\cos^2\Phi e^{-iE_2t_p}\right.\right.\\&\left.\left.+\sin^2\Phi e^{-iE_3t_p}\right)\right]\left[\frac{1}{4}\left(\cos\left(\frac{\beta}{2}\right)+1\right)\left(\cos\left(\frac{\beta}{2}\right)-1\right)\left(e^{iE_1t_p}+e^{iE_4t_p}\right)-\frac{1}{2}\sin^2\left(\frac{\beta}{2}\right)\left(\cos^2\Phi e^{iE_2t_p}+\sin^2\Phi e^{iE_3t_p}\right)\right]\\&-\left[\frac{1}{4}\left(\cos\left(\frac{\beta}{2}\right)+1\right)\left(\cos\left(\frac{\beta}{2}\right)-1\right)\left(e^{-iE_1t_p}+e^{-iE_4t_p}\right)-\frac{1}{2}\sin^2\left(\frac{\beta}{2}\right)\left(\cos^2\Phi e^{-iE_2t_p}+\sin^2\Phi e^{-iE_3t_p}\right)\right]\\&\times\left[\frac{1}{4}\left(\cos\left(\frac{\beta}{2}\right)-1\right)^2 e^{iE_1t_p}+\frac{1}{4}\left(\cos\left(\frac{\beta}{2}\right)+1\right)^2 e^{iE_4t_p}-\frac{1}{2}\sin^2\left(\frac{\beta}{2}\right)\left(\cos^2\Phi e^{iE_2t_p}+\sin^2\Phi e^{iE_3t_p}\right)\right]\Bigg\}.\end{aligned} \tag{31}$$

Here, β and t_p are the nominal flip angle and duration, respectively, of the first pulse, Φ is defined in Eq. (B10), and E_i are the eigenvalues of the spin Hamiltonian [cf. Eq. (1)] in its eigenbasis. These eigenvalues are given in Eq. (B13). Hence a double quantum coherence exists after the first pulse.

In Fig. 4 we plot the efficiency of coherence transfer $0\to 2$, denoted by $T_{0\to 2}$, calculated using Eqs. (B15) and (C7) and an n of 16, as a function of the length of the first pulse, t_p and the strength of its irradiating field, B_1. Since the double quantum coherence following this pulse arises due to perturbative contributions of the dipolar interaction during this pulse, the details of this transfer were found to depend in general on this interaction. However, the plot shown is representative of dipolar couplings smaller than 4.4 G ($r=18.5$ Å). The maximum transfer efficiency, $T_{0\to 2}$ is about 6%–10% of the maximum single quantum transfer efficiency, $T_{0\to 1}$, depending on the strength of the dipolar interaction. The bands of optimum double quantum transfer lie along ridges in the B_1-t_p plane. However, note that relaxation has been neglected during the pulse. This would be significant for the long pulses needed to generate the double quantum coherence.

We now turn to the efficiency of back coherence transfer, i.e., $T_{2\to -1}$. For the double quantum coherence, $T_{2\to -1}$, is given by

$$T_{2\to -1}=R^2_{21}P^2_{41}+R^2_{31}P^2_{41}+R^2_{41}P^2_{42}+R^2_{41}P^2_{43}. \tag{32}$$

In Fig. 5 we plot $T_{2\to -1}$ as a function of the duration, t_p, and strength, B_1 of the second pulse. The double quantum transfer is again about 6%–10% as efficient as the single quantum transfer, depending on the strength of the dipolar interaction.

The DQ signal for a given orientation of the dipolar vector is given by

$$\begin{aligned}F^{\mathrm{DQ}}(t_1,t_2)=(R^1_{11}P^1_{14}-R^1_{14}P^1_{44})[&S^2_1{}^*R^2_{21}P^2_{41}+S^2_2{}^*R^2_{31}P^2_{41}\\&+S^2_3{}^*R^2_{41}P^2_{42}+S^2_4{}^*R^2_{41}P^2_{43}]e^{3i\phi^2}e^{-2i\phi^1}\\&\times e^{-i(E_1-E_4)t_1}e^{-t_1/T^D_2}e^{-t_2/T^S_2}e^{-2\pi^2\Delta^2_G(t_2-2t_1)^2}.\end{aligned} \tag{33}$$

The single quantum terms present during t_2 appear in S^2_j ($j=1,2,3,4$). Note, that in Eq. (33) inhomogeneities are refocused at $t_2=2t_1$. The extra factor of 2 [compare Eq. (33) with Eq. (27) where they refocus at $t_2=t_1$] reflects the fact that static inhomogeneities affect the double quantum coherence doubly.[22,37] The full rigid limit double quantum powder signal is obtained by integrating Eq. (33) over a unit sphere using Eq. (26).

In Figs. 6 and 7 we show the theoretical two pulse double quantum powder spectra obtained for a biradical for a range of dipolar interactions. For typical values of the maximum irradiation field (i.e., $B_1=17.8$ G) the double quantum spectrum shows little dependence on the strength of the dipolar interaction (figure not shown). Using Figs. 4 and 5 as reference we considered the behavior of the two pulse DQ signal for four cases: (a) pulses of length 5 ns and strength 15.8 G, (b) pulses of length 5 ns and strength 1.8 G, (c) pulses of length 80 ns and strength 1.8 G (i.e., located on the

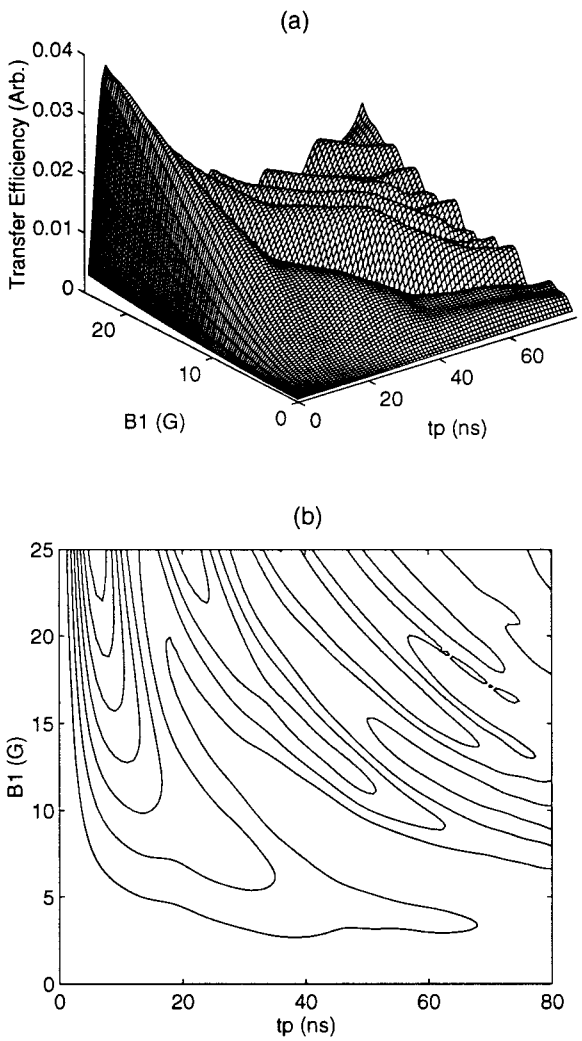

FIG. 4. The transfer of $0 \rightarrow 2$ coherence during an arbitrary first pulse of duration, t_p and irradiation strength, B_1, in the two pulse double quantum experiment. Both (a) magnitude and (b) contour plots are shown. The value of Trotter exponent, n, was 16. The value of D was 4.4 G ($r=18.5$ Å). Other simulation parameters are $\beta_1=\beta_2=120°$, The other Euler angles needed to define the PAS were $\alpha_1=\alpha_2=\gamma_2=0°$. The magnetic parameters are $g_{xx}=2.0086$, $g_{yy}=2.0066$, $g_{zz}=2.0032$ and $A_{xx}=A_{yy}=6.23$ and $A_{zz}=35.7$. Note that relaxation has been neglected during the pulse. The carrier frequency of the pulse is 9.32 GHz and is equal to the center frequency given by $g_s\beta_e B_0/h$ where $g_s=\frac{1}{3}\Sigma_i g_{ii}$. The maximum transfer efficiency of 0.07 occurs at $B_1=93.5$ G and $t_p=1$ ns. However, the maximum sensitivity to modulation from the dipolar interaction occurs for smaller B_1 and larger t_p (cf. the text).

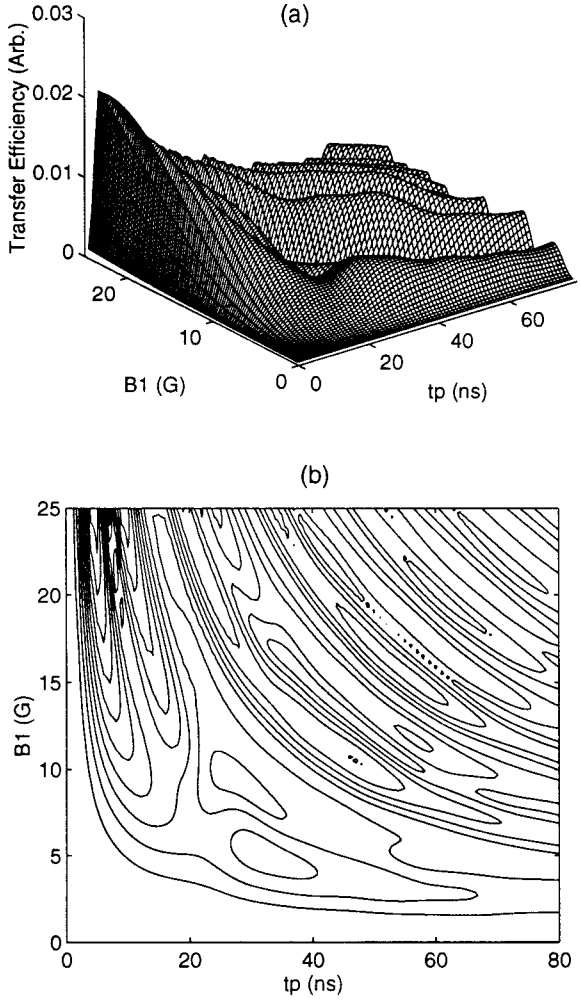

FIG. 5. The transfer of $2 \rightarrow -1$ coherence during an arbitrary second pulse of duration, t_p and irradiation strength, B_1, in the two pulse double quantum experiment. Both (a) magnitude and (b) contour plots are shown. The value of Trotter exponent, n, was 16. The value of D was 4.4 G ($r=18.5$ Å). Other simulation parameters are the same as in Fig. 4. Note that relaxation has been neglected during the pulse. The carrier frequency of the pulse is 9.32 GHz and is equal to the center frequency given by $g_s\beta_e B_0/h$, where $g_s=\frac{1}{3}\Sigma_i g_{ii}$. The maximum transfer efficiency of 0.03 occurs at $B_1=126.5$ G and $t_p=2$ ns. However, the maximum sensitivity to modulation from the dipolar interaction occurs for smaller B_1 and larger t_p (cf. the text).

first ridge in Figs. 4 and 5), and (d) pulses of length 80 ns and strength 15.8 G. For cases (a) and (b) the double quantum spectrum showed little dependence on the dipolar interaction (figures not shown). Also for case (d) the spectrum shows only a small dependence on the dipolar interaction. This is apparent in Fig. 6 where the maximum of the echo (i.e., along $t_2=2t_1$) appears at a longer value of t_2 as the dipolar interaction decreases. Such a dependence becomes dramatic for a weak pulse of strength 1.8 G at a center resonance frequency of 9.32 GHz. (cf. Fig. 7) and length 80 ns [case (c)]. The stronger the dipolar interaction, the faster is the modulation of the echo along the $t_2=2t_1$ axis in Fig. 7. Therefore, a long weak pulse is required for the effective creation of a modulation pattern in the time domain, from which the dipolar interaction can be obtained. However, note that the maximum intensity of the signal with $B_1=1.8$ G and pulse length 80 ns [case (c)] is smaller by a factor of 1–5 (depending on the dipolar interaction) when compared to that with $B_1=15.8$ G and pulse length 80 ns. [case (d), cf. Fig. 6 vs Fig. 7]. Thus one must give up signal-to-noise in order to generate DQ signals that are sensitive to the modulation pattern due to the dipolar interaction. The maximum intensity of a two pulse DQ signal for case (c), from simulations, with $D=10$ G ($r=14.1$ Å) [cf. Fig. 7(a)] was found to be about a factor of 9 weaker when compared to that of a COSY experiment calculated using Eq. (27) (with $B_1=15.8$ G and pulse lengths of 5 ns). For a smaller dipolar interaction of 1

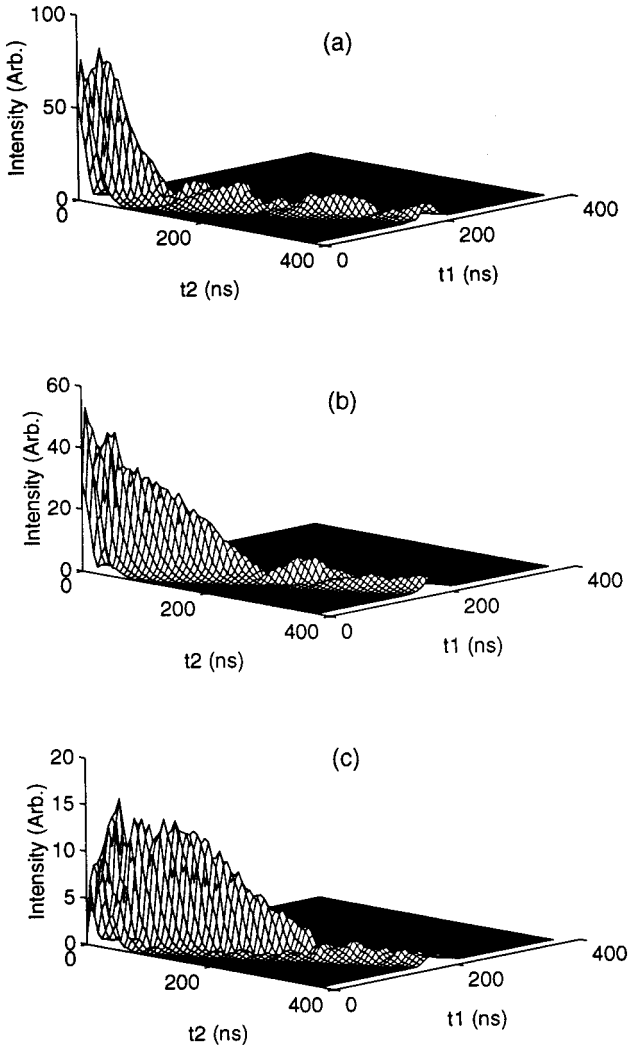

FIG. 6. Theoretical two pulse DQ spectra for biradical with a dipolar interaction, D, of (a) 10 G ($r=14.1$ Å), (b) 5 G ($r=17.8$ Å), and (c) 1 G ($r=30.3$ Å). The strength of the irradiation field, B_1, was 15.8 G and the lengths of the pulses were 80 ns each. The relaxation parameters were: $T_2^S=500$ ns, $T_2^D=200$ ns, and $\Delta_G=2.0$ G. The remaining parameters are the same as in Fig. 4.

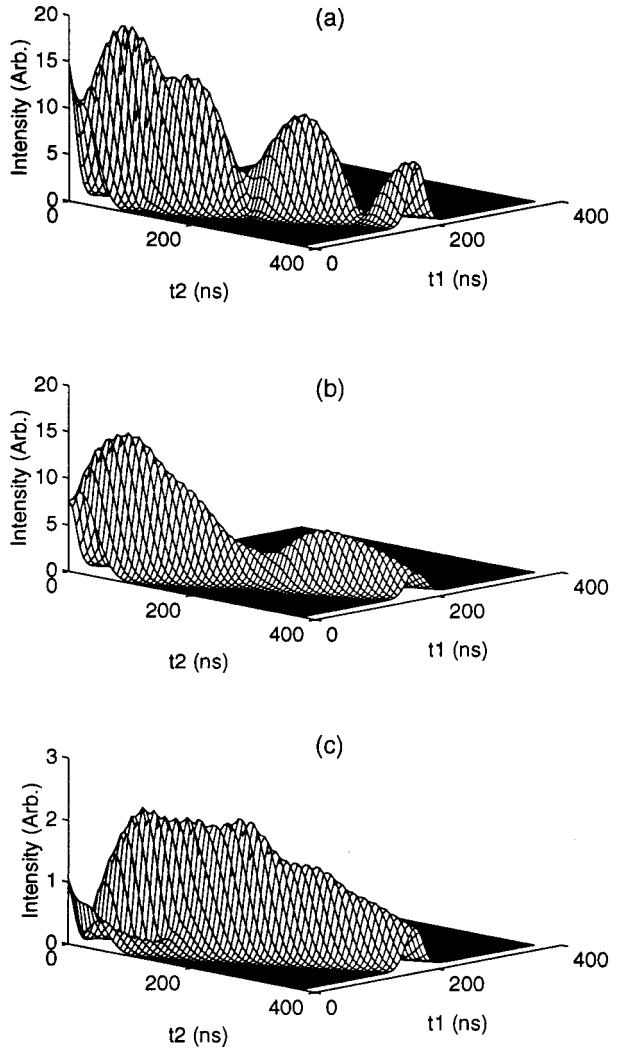

FIG. 7. Theoretical two pulse DQ spectra for biradical with a dipolar interaction, D, of (a) 10 G ($r=14.1$ Å), (b) 5 G ($r=17.8$ Å), and (c) 1 G ($r=30.3$ Å). The strength of the irradiation field, B_1, was 1.8 G and the lengths of the pulses were 80 ns. The relaxation parameters were: $T_2^S=500$ ns, $T_2^D=200$ ns, and $\Delta_G=2$ G. The remaining parameters are the same as in Fig. 4.

G ($r=30.3$ Å) the signal intensity of the DQ experiment was about 70 times weaker compared to the COSY signal. However, we have not tried to find the precise optimum conditions for this experiment.

In Fig. 8 we show two DQ powder spectra, obtained using a long weak pulse, with the same value of the dipolar interaction (2.5 G, $r=22.2$ Å) but with different geometries of the biradical (i.e., different values of β_1 and β_2, cf. Fig. 1). While the modulation frequency, which reflects the dipolar interaction, is largely unchanged the modulation pattern depends on the biradical geometry. This remarkable feature is potentially very useful for structural studies.

We postpone until the next section the discussion of why such a sensitivity towards the structural properties (i.e., the interelectron distance and biradical geometry) arises. However, we note that Larsen and Singel[9] obtained a similar sensitivity towards geometrical constraints in their weak pulse DEER experiments.

IV. FIVE PULSE SIGNALS: DQM AND DQ-COSY

We now turn to the five pulse sequence used to detect double quantum coherence.[1] The first pulse creates transverse single quantum magnetization (± 1 coherences) which evolves for a period t_1. The spins get labeled with the dipolar frequency during this interval [i.e., $T_{1,\pm 1}\rightarrow T_{2,\pm 1}$ in irreducible spherical tensor operators (ISTO) notation, cf. below]. A second pulse transfers this magnetization to z magnetization (longitudinal as well as 0 quantum coherences). During the period t_2 the system decays with a rate given by T_1. Magnetization transfer can also occur during this period, which can lead to cross peaks in the 2D spectrum, in analogy to the 2D ELDOR ESR experiment.[25] We have neglected the magnetization transfer in this discussion. This is justified below. At the end of t_2 a third pulse transfers the z magnetization to transverse double quantum magnetization (± 2 coherences). In principle, this is a forbidden

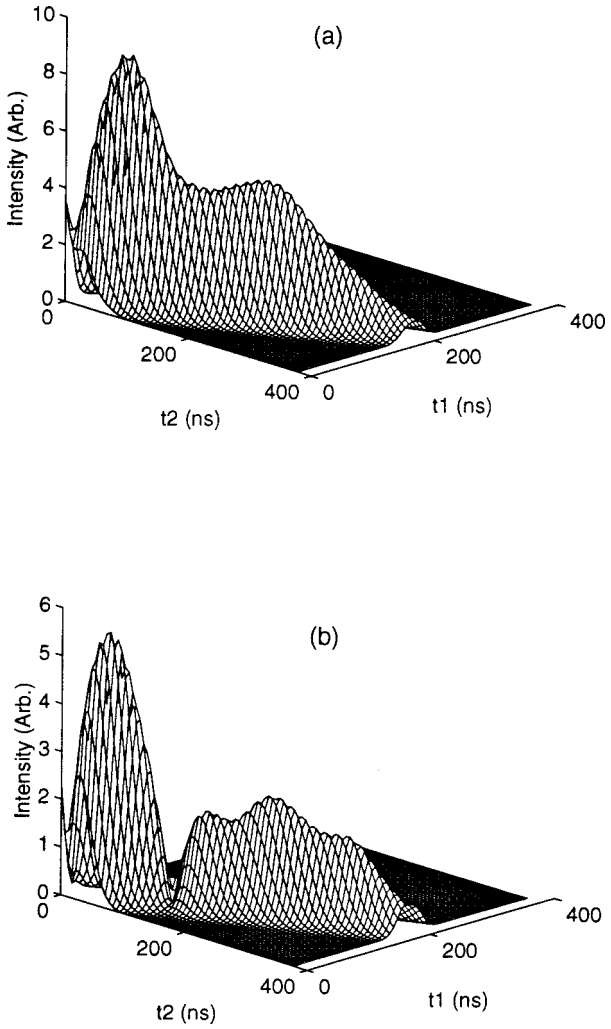

FIG. 8. Theoretical two pulse DQ spectra for biradical with a dipolar interaction, D, of 2.5 G ($r=22.2$ Å) and geometry (a) $\beta_1=\beta_2=120°$ and (b) $\beta_1=30°$, $\beta_2=120°$. The strength of the irradiation field, B_1, was 1.8 G and the lengths of the pulses were 80 ns each. The relaxation parameters were: $T_2^S=500$ ns, $T_2^D=200$ ns, and $\Delta_G=2.0$ G. The remaining parameters are the same as in Fig. 4.

transition,[35,36] and it occurs due to the arbitrary nature of the third pulse. Since the double quantum coherence rapidly decays away due to inhomogeneous broadening (cf. Sec. III) a refocusing pulse is necessary. Hence a π pulse is applied, after a period, t_3, and the system evolves for a time t_4 under a refocused inhomogeneity (i.e., the order of the coherences is reversed and we obtain ∓ 2). At the end of t_4 a fifth pulse transfers the double quantum coherences to observable single quantum coherences which are detected in t_5.

To summarize, the two coherence pathways that lead to a formation of an echo at $t_5 \approx t_1$ are given by

$$\text{(i)}\quad 0 \overset{P_1}{\rightarrow} +1 \overset{P_2}{\rightarrow} 0 \overset{P_3}{\rightarrow} +2 \overset{P_4}{\rightarrow} -2 \overset{P_5}{\rightarrow} -1: \quad F_a$$

and

$$\text{(ii)}\quad 0 \overset{P_1}{\rightarrow} +1 \overset{P_2}{\rightarrow} 0 \overset{P_3}{\rightarrow} -2 \overset{P_4}{\rightarrow} +2 \overset{P_5}{\rightarrow} -1: \quad F_b. \tag{34}$$

This pulse sequence is shown in Fig. 3(c). For the desired signal, then, the double quantum coherence is refocused by the fourth pulse. Single quantum coherence that decays due to inhomogeneous broadening in t_1 is refocused along t_5, and hence the signal forms at $t_5 \approx t_1$. Alternatively pathways (i) and (ii) can be written in irreducible spherical tensor operator (ISTO) formalism[22,38,39]

$$T_{10} \overset{P_1}{\rightarrow} T_{1+1} \overset{t_1}{\rightarrow} T_{2+1} \overset{P_2}{\rightarrow} T_{20} \overset{t_2}{\rightarrow} T_{20} \overset{P_3}{\rightarrow} T_{2\pm 2} \overset{t_3}{\rightarrow} T_{2\pm 2} \overset{P_4}{\rightarrow} T_{2\mp 2} \overset{t_4}{\rightarrow} T_{2\mp 2} \overset{P_5}{\rightarrow} T_{2\mp 1} \overset{t_5}{\rightarrow} T_{1-1}. \tag{34a}$$

Note that the $T_{10} \overset{\pi/2}{\rightarrow} T_{1-1}$ pathway would be ''FID-like'' and would decay away in the dead time after the fifth pulse. Hence it is not included. While these ISTO's refer only to a coupled two electron system, they serve to label the coherences more explicitly. For example, the T_{2+1} coherence grows in t_1 from T_{1+1} due to the interelectron interaction.[40] It is this coherence which provides the double quantum signal. Such detail is lacking in the simple coherence pathway picture. On the other hand, the ISTO formalism fails to identify the precise terms, in product operator notation, that are the desired ones in each step.

We now justify our neglect of magnetization transfer during t_2. In the incipient rigid limit, the duration t_2 for a double quantum ESR experiment is typically 50–250 ns (for interelectron distances of about 20–30 Å). At very slow motional rates the cross-relaxation processes that lead to a magnetization transfer would be ineffective in creating substantial cross peaks during such a short duration. In fact, we were unable to obtain cross peaks, even in the 2D ELDOR experiments, at the very slow motional rates characterizing the samples and temperatures studied. Hence it is safe to neglect magnetization transfer for the moment.

Note that in the actual experiments the relation between t_1 and t_2 is fixed as is the relation between t_3 and t_4 (i.e., $t_1=t_2$ and $t_3=t_4$). Saxena and Freed[1] thus defined t_1 (and t_2) as t_p and t_3 (and t_4) as t_1. We have deliberately differentiated each time interval so that the final equations reflect the details of the coherence pathway more clearly.

Two kinds of double quantum experiments are relevant with this five pulse sequence.[1] In the double quantum modulation (DQM) experiment the intervals, t_3 and t_4 (with $t_3=t_4$) are kept fixed. The intervals, $t_1=t_2$ are stepped out. Coherences that lead to the formation of the double quantum signal grow in during the period t_1.[40] These coherences depend entirely on the presence of an interelectron interaction (i.e., the dipolar and/or exchange interaction). The modulation of the signal as a function of t_1 therefore depends on the strength of the dipolar interaction (or exchange interaction) and hence this experiment is useful for the measurement of the interelectron distance. In double quantum-COSY (DQ-COSY), the intervals, $t_1=t_2$ are kept fixed and the signal is measured as a function of t_5 for a series of steps in the double quantum evolution periods, $t_3=t_4$. This experiment provides the homogeneous double quantum relaxation rate, T_2^D.

The signals due coherence pathways (i) and (ii) in Eq. (34) are denoted by F_a and F_b, respectively. These are given by

$$F_a(t_1,t_2,t_3,t_4,t_5) = e^{-i\phi^1}e^{i\phi^2}e^{2i\phi^3}e^{-4i\phi^4}e^{3i\phi^5} \times e^{-i(E_1-E_4)t_4}e^{-i(E_4-E_1)t_3}R_{14}^4P_{14}^4 \times e^{-t_3/T_2^D}e^{-t_4/T_2^D}\sum_{i=1}^{i=4} e^{-t_1/T_2^S}M_{ia} \times e^{-t_2/T_1}N_{ia}\sum_{j=1}^{j=4} e^{-t_5/T_2^S}Q_{ja} \quad (35)$$

and

$$F_b(t_1,t_2,t_3,t_4,t_5) = e^{-i\phi^1}e^{i\phi^2}e^{-2i\phi^3}e^{4i\phi^4}e^{-i\phi^5} \times e^{-i(E_4-E_1)t_4}e^{-i(E_1-E_4)t_3}R_{41}^4 \times P_{41}^4e^{-t_3/T_2^D}e^{-t_4/T_2^D}\sum_{i=1}^{i=4} e^{-t_1/T_2^S} \times M_{ib}e^{-t_2/T_1}N_{ib}\sum_{j=1}^{j=4} e^{-t_5/T_2^S}Q_{jb}. \quad (36)$$

Here, the superscripts on R, P, and ϕ denote the number of the pulse, while the subscripts on R and P refer to the actual matrix elements. The terms in M, N, and Q are provided in Appendix D. Again, assuming that the inhomogeneous broadening is given by a Gaussian distribution, the signal can be written as

$$F_+^5 = (F_a + F_b)e^{-2\pi^2\Delta_G^2(t_1-t_5)^2}, \quad (37)$$

where Δ_G is the Gaussian inhomogeneous broadening parameter in frequency units.

In Fig. 9 we show a theoretical time domain DQM powder spectrum obtained using Eqs. (37) and (26), for an interelectron distance of 14.1 Å, as a stack plot. The maximum of the time domain signal, from the coherence pathways (i) and (ii), is expected to occur along the $t_5=t_1$ axis (cf. above). However, in practice the finiteness of the pulses causes the center of gravity of the echo to shift slightly (i.e., a few nanoseconds) from an exact $t_5=t_1$ behavior. Fortunately, this is no problem in the 2D format! From theoretical simulations, we find that this shift also depends on the strength of the dipolar interaction. This seems reasonable as the perturbative contributions of the dipolar interaction during the third pulse lead to the formation of the double quantum signal.[1] Note the oscillatory behavior of the echo maximum as a function of t_1. It is these oscillations that provides the strength of the dipolar interaction.

This is demonstrated more clearly in Fig. 10 where a single slice of the 2D time domain spectrum is plotted. Here, the echo maximum as a function of t_1 is shown for theoretical simulations of the DQM experiment for different values of the dipolar interaction [$D=10$ G ($r=14.1$ Å), $D=2$ G ($r=24$ Å), and $D=1.0$ G $r=38$ Å]. The stronger the dipolar interaction the faster the coherence grows to a maximum, and the greater is the frequency of the oscillations. This is a remarkable feature as the dipolar interaction is very small when compared to the dominant g and hf terms. Also, for a powder one would expect that the $(3\cos^2\theta-1)$ dependence of the dipolar interaction [cf. Eq. (3)] would lead to a smearing out of this oscillation. However, the DQM signal is very sensitive to the dipolar interaction for the coherence pathway of Eq. (34a) because of an orientational selectivity, i.e., the signal is mainly from those molecules with orientations of the dipolar vector predominantly along the dc magnetic field.[1]

This feature of orientational selectivity is in fact appropriate for this type of a forbidden transition. Heuristically this can be rationalized by using a simplified Hamiltonian, i.e.,

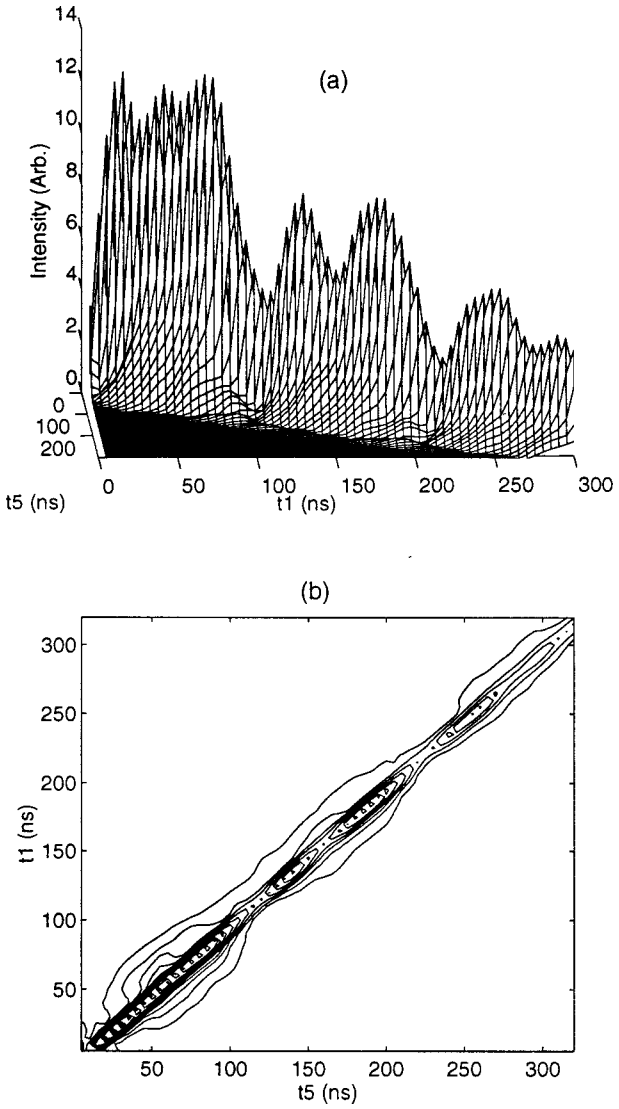

FIG. 9. Theoretical DQM spectra for biradical with a interelectron distance, r of 14.1 Å, shown in (a) stack plot; (b) contour plot. The simulation parameters are $D=10$ G, $\beta_1=180°$, $\beta_2=150°$, $T_2^S=500$ ns, $T_2^D=300$ ns, and $\Delta_G=2$ G. The strength of the irradiation field, B_1, was 15.8 G. The duration of the pulses were: $P_1=P_3=P_5=5$ ns and $P_2=P_4=10$ ns. The other parameters were the same as in Fig. 4.

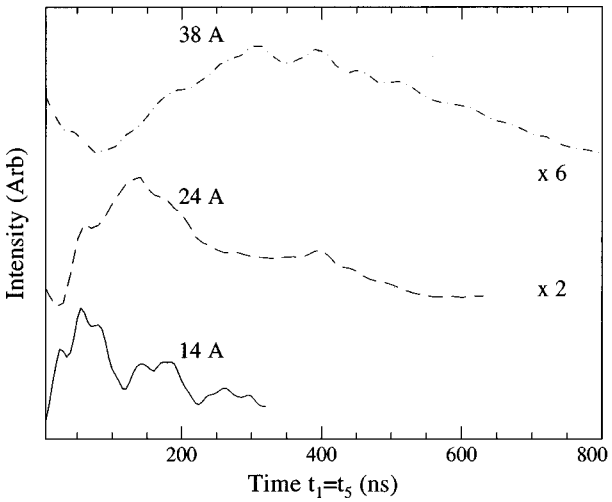

FIG. 10. Theoretical DQM spectra for biradical with a interelectron distance, (a) $r=14.1$ Å, $D=10$ G (solid line —), (b) $r=24$ Å, $D=2$ G (dashed line- -), and (c) $r=38$ Å, $D=0.5$ G (dash–dot line —·—). The echo maximum for each value of t_1 is shown as a function of t_1. In these simulations $\beta_1=180°$ and $\beta_2=150°$. The relaxation parameters were: $T_2^S=500$ ns, $T_2^D=300$ ns, and $\Delta=2$ G. The strength of the irradiation field, B_1, was 15.8 G. The duration of the pulses were $P_1=P_3=P_5=5$ ns and $P_2=P_4=10$ ns. Other simulation parameters are the same as in Fig. 4. The maximum of the echo as a function of t_1 is shown.

$$H_s=\Omega_1 S_{z_1}+\Omega_2 S_{z_2}+bS_{z_1}S_{z_2}, \tag{38}$$

where

$$b\propto D(3\cos^2\theta-1). \tag{39}$$

This was the Hamiltonian used in Ref. 1 to justify the creation of a forbidden double quantum coherence, using product operator techniques.[40] For simple Hamiltonians (i.e., composed of commuting terms) the product operator formalism provides a method for easy visualization in terms a simple vector picture of the effect of the pulses and evolution in a complex pulse sequence. The ISTO formalism while more powerful does not carry this advantage.

The key feature is the creation of the double quantum coherence [i.e. $(S_{x_1}S_{y_2}+S_{x_2}S_{y_1})$] in product operator formalism] from zero quantum coherences (i.e., $S_{z_1}S_{z_2}$) during the third pulse of duration, P_3 [cf. Fig. 11(a)]. The lowest order split Hamiltonian theory expansion of this pulse is shown in Fig. 11(b). It consists of two nonselective pulses of duration $P_3/2$ each, with a period of free evolution of duration, P_3, in between. The first of these nonselective ''half-pulses'' yields, using product operator formalism, $(S_{z_1}S_{y_2}+S_{z_2}S_{y_1}\equiv\mathbf{A})$. During free evolution under the Hamiltonian given by Eq. (38) this provides the term $(S_{z_1}S_{x_2}+S_{z_2}S_{x_1}\equiv\mathbf{B})$, which is transferred to double quantum coherence by the second ''half-pulse.'' **B** grows in as $\sin(bP_3/2)$, from **A**, during the period of ''apparent'' free evolution, P_3, and hence only those orientations ($b\propto 3\cos^2\theta-1$) which can maximize this transfer would be selectively pumped to the double quantum coherence. This leads to the orientational selectivity.

In the real nitroxide biradical, the presence of large g and hf terms would tend to detract from this simple selectivity, (i.e., from the growth of term **B**), providing the challenge to obtaining the double quantum signal. In fact, one would also expect that the detailed modulation pattern would be affected by orientations of the nitroxide g and hf tensors with respect to one another, since the degree to which the resonant shifts provided by the g and hf tensors lead to different resonant frequencies for the electron spins is a measure of their distinguishability, and hence of the failure of simple singlet–triplet representation for them. This is indeed found to be the case, as is shown in Fig. 12 which shows theoretical simulations with the same dipolar interaction (10 G, $r=14.1$ Å) but different geometries of the biradical, (i.e., different β_1 and β_2 in Fig. 1). While the modulation frequency (which reflects the dipolar interaction) remains largely unchanged, the exact shape of the modulation pattern depends on the orientations of the nitroxides with respect to each other. Note the intensities of the first three maxima along the $t_5=t_1$ axis are different for the two orientations. Thus the orientational selectivity also provides structural sensitivity. Hence this experiment is potentially very important for structural studies in labeled peptides or proteins, for example.

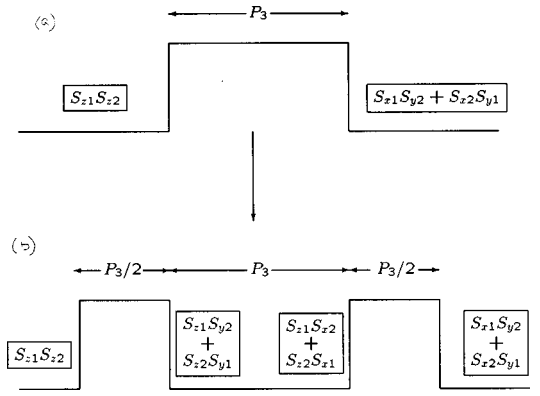

FIG. 11. Generation of forbidden double quantum coherence during third pulse (a) the third pulse with relevant product operator terms and (b) lowest order expansion in split Hamiltonian theory for the third pulse.

The presence of such orientational selectivity due to the first pulse in the two pulse DQ experiment (cf. last section) results in its sensitivity towards the dipolar interaction (cf. Fig. 7) and biradical geometry (cf. Fig. 8). In this sequence the first pulse causes the transfer $(S_{z_1}+S_{z_2}\rightarrow S_{x_1}S_{y_2}+S_{x_2}S_{y_1})$ in the product operator formalism. The lowest order split Hamiltonian theory approximation corresponds to the case provided in Slichter's monograph.[40] The first ''half-pulse'' creates $(S_{y_1}+S_{y_2}\equiv\mathbf{C})$ and during ''apparent'' free evolution $(S_{x_1}S_{z_2}+S_{x_2}S_{z_1}\equiv\mathbf{D})$ is created from **C**, which is transferred to the double quantum coherence by the second ''half-pulse.'' Again, **C** grows in as $\sin(aP_1/2)$ from B and as before this sinusoidal ''weighting'' provides the orientational selectivity.

However, note that the spin system in the two pulse sequence is ''prepared'' differently [it exist as $(S_{z_1}+S_{z_2})$] before the excitation to the double quantum coherence than in the five pulse sequence. In the five pulse sequence the term excited to the double quantum coherence (cf. above)

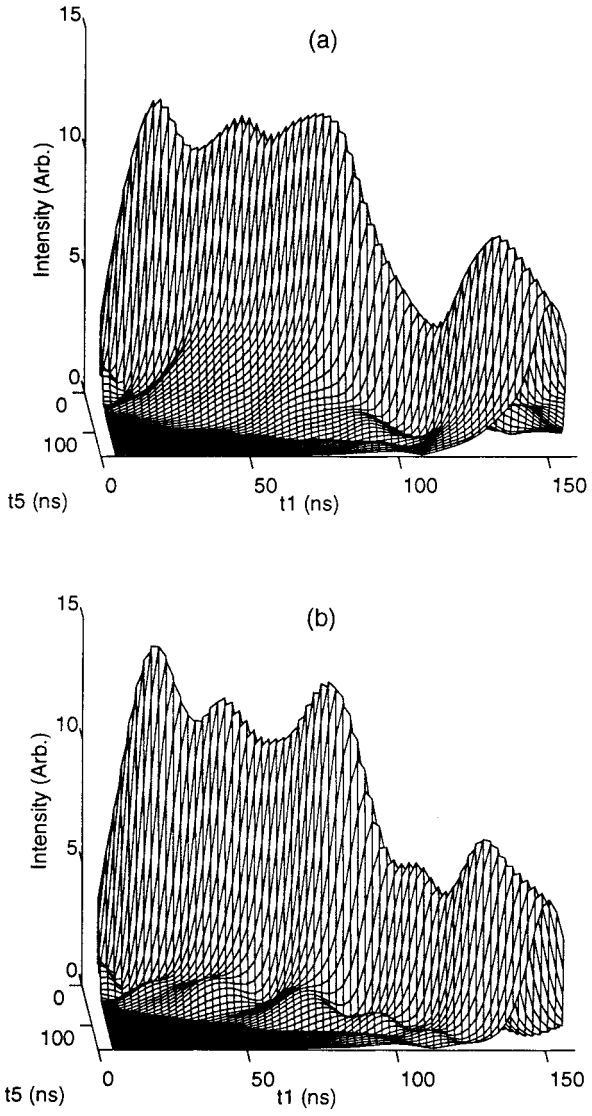

FIG. 12. Theoretical DQM spectra for two orientations of a biradical with an interelectron distance of 14.1 Å ($D=16$ G). (a) $\beta_1=180°$, $\beta_2=150°$ and (b) $\beta_1=180°$, $\beta_2=120°$. The relaxation parameters were: $T_2^S=500$ ns, $T_2^D=300$ ns, and $\Delta=2$ G. The duration of the pulses were $P_1=P_3=P_5=5$ ns and $P_2=P_4=10$ ns and the strength of the irradiation field, B_1, was 15.8 G. The other parameters are the same as in Fig. 4.

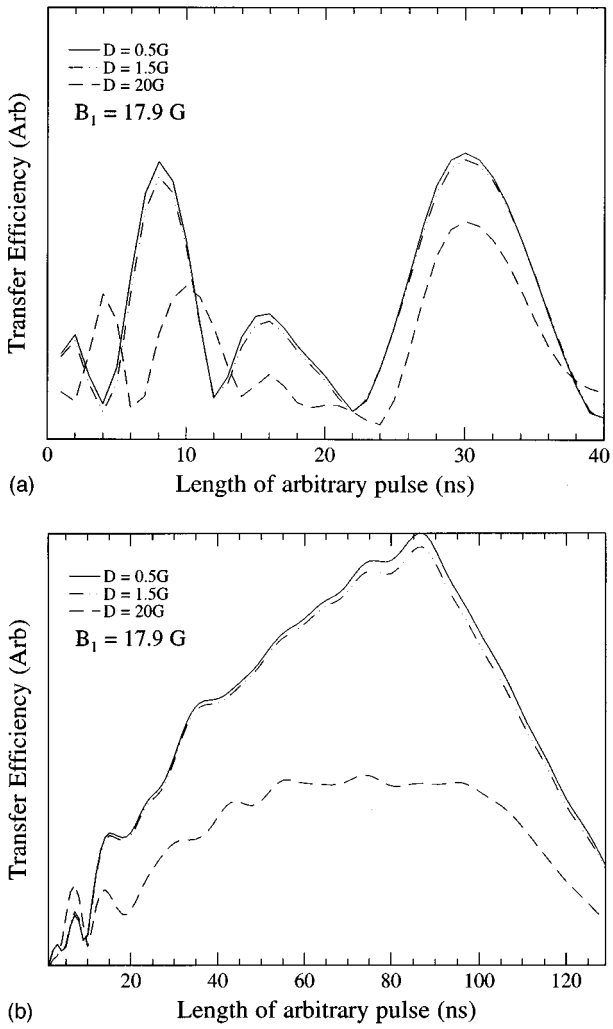

FIG. 13. The transfer of $m\rightarrow p$ coherence ($p=1,2$) during an arbitrary pulse of duration, t_p, in the five pulse sequence [cf. Fig. 3(c)]. The irradiation irradiation strength, B_1, was 17.9 G. These are shown for three different values of the dipolar interaction: $D=0.5$ G ($r=38$ Å solid —), $D=1.5$ G ($r=26.5$ Å dash–dot–dot —··) and $D=20$ G ($r=11.2$ Å dashed - -). Simulations show the effect of (a) the second pulse ($m=+1$, $p=0$) and (b) the third pulse ($m=0$ and $p=\pm 2$) in the five pulse sequence. The value of Trotter exponent, n, was 8. Other simulation parameters are the same as in Fig. 4. Note that relaxation has been neglected during the pulse.

comes labeled with the dipolar frequency during the interval t_1. This could account in part for the reason why the first pulse of the two pulse sequence needs to be weaker (i.e., $B_1=1.8$ G) to fully exhibit orientational selectivity.

The maximum signal intensity of the five pulse experiment (cf. Fig. 10), from simulations, when compared to the COSY experiment, is weaker by a factor of 14 (for $D=10$ G, $r=14.1$ Å) to 60 (for $D=1$ G, $r=30.3$ Å). Again, we have not tried to find the precise optimum conditions for this experiment. But given our results so far, the signal intensity of the five pulse DQ experiment is similar to the two pulse DQ experiment (cf. Sec. III B). The latter is, in principle, a simpler experiment, since it involves only two pulses and a smaller number of possible coherence pathways.

Finally, we would like to examine the features of the effects of the second and third pulses on the double quantum pathway. The detailed expressions, while unwieldy, can be easily extracted from Eqs. (D1)–(D4) in Appendix D. In Fig. 13(a) we show the transfer of $+1\rightarrow 0$ coherence due to the second pulse in the five pulse sequence. For a B_1 of about 17.9 G the optimum pulse length is about 8 ns. Figure 13(b) shows the transfer $0\rightarrow\pm 2$ due to the third pulse. For optimum transfer the pulse should be of 40–100 ns duration. These optimum pulse durations are largely independent of the dipolar interaction, for a range of distance from 15 to 40 Å. Using these optimum pulse durations in simulations we find we should be able to increase the signal by a factor of 2–3 over that obtained previously.[1]

V. SIX PULSE SIGNALS: REFOCUSED PRIMARY DOUBLE QUANTUM ECHO

Finally, we would like to discuss the feasibility of primary double quantum echoes in the rigid limit. The success

of the double quantum experiments discussed so far relies on the creation of extra coherences by arbitrary pulses. One would *a priori* (and mistakenly!) assume such effects to be weak compared to the primary echoes. What about the primary double quantum signal from a three pulse sequence,[40] one might ask? In this sequence the first (nominal $\pi/2$) pulse creates $x-y$ magnetization (± 1 coherences) which evolve for a period, t_a during which they are labeled with the dipolar frequency. A second (nominal $\pi/2$) pulse creates the double quantum coherence which is transferred to observable single quantum magnetization after a time t_b, by a third pulse. Large inhomogeneities in typical ESR samples would make this experiment, in its current form, difficult. Hence, one would insert π pulses in between the periods t_a and t_b, to refocus single and double quantum coherences, respectively (cf. Ref. 26 a for the case of NMR). The signal after this modified five pulse sequence would be FID-like, and hence it would rapidly decay away in the dead time after the fifth pulse. Therefore, one would need to incorporate a sixth pulse to refocus the FID into an echo.

The signal, then consists of contributions from the following coherence pathways:

$$0 \overset{P_1}{\rightarrow} -1 \overset{P_2}{\rightarrow} +1 \overset{P_3}{\rightarrow} -2 \overset{P_4}{\rightarrow} +2 \overset{P_5}{\rightarrow} +1 \overset{P_6}{\rightarrow} -1: \quad F_{6a},$$

$$0 \overset{P_1}{\rightarrow} -1 \overset{P_2}{\rightarrow} +1 \overset{P_3}{\rightarrow} +2 \overset{P_4}{\rightarrow} -2 \overset{P_5}{\rightarrow} +1 \overset{P_6}{\rightarrow} -1: \quad F_{6b},$$

$$0 \overset{P_1}{\rightarrow} +1 \overset{P_1}{\rightarrow} -1 \overset{P_1}{\rightarrow} +2 \overset{P_1}{\rightarrow} -2 \overset{P_1}{\rightarrow} +1 \overset{P_1}{\rightarrow} -1: \quad F_{6c},$$

$$0 \overset{P_1}{\rightarrow} +1 \overset{P_1}{\rightarrow} -1 \overset{P_1}{\rightarrow} -2 \overset{P_1}{\rightarrow} +2 \overset{P_1}{\rightarrow} +1 \overset{P_1}{\rightarrow} -1: \quad F_{6d}. \tag{40}$$

Alternatively, in terms of ISTO's of a coupled two electron spin system these coherence pathways are described as

$$T_{10} \overset{P_1}{\rightarrow} T_{1\pm1} \overset{t_1}{\rightarrow} T_{2\pm1} \overset{P_2}{\rightarrow} T_{2\mp1} \overset{t_2}{\rightarrow} \left[T_{2\mp1} \overset{P_3}{\rightarrow} T_{2\pm2} \right] \overset{t_3}{\rightarrow} T_{2\pm2} \overset{P_4}{\rightarrow} T_{2\mp2} \overset{t_4}{\rightarrow} T_{2\mp2} \overset{P_5}{\rightarrow} T_{2\mp1} \overset{t_5}{\rightarrow} T_{1\mp1} \overset{P_6}{\rightarrow} T_{1\pm1} \overset{t_6}{\rightarrow} T_{1-1}, \tag{40a}$$

where we set $t_1=t_2$, $t_3=t_4$, with the echo at $t_6=t_5$. Also the most effective sequence would consist of a nominal $\pi/2\rightarrow\pi\rightarrow\pi/2\rightarrow\pi\rightarrow\pi/2\rightarrow\pi$ sequence (i.e., $P_1=P_3=P_5=\pi/2$ and $P_2=P_4=P_6=\pi$). The large brackets around $T_{2\mp1} \overset{P_3}{\rightarrow} T_{2\pm2}$ indicate that all coherence transfers need to be included, i.e., $T_{2-1} \overset{P_3}{\rightarrow} T_{2-2}$ and $T_{2+1} \overset{P_3}{\rightarrow} T_{2+2}$ are also relevant. Also, the T_{1-1} coherence created by the first pulse (and refocused by the second) contributes to the DQ echo.

These signals from the coherence pathways F_{6a} to F_{6d} given by Eq. (40), for each orientation are given by

$$\begin{aligned} F_{6a}(t_1,t_2,t_3,t_4,t_5,t_6) &= e^{i\phi^1} e^{-2i\phi^2} e^{3i\phi^3} e^{-4i\phi^4} e^{i\phi^5} e^{2i\phi^6} e^{-i(E_1-E_4)t_4} \\ &\times e^{-i(E_4-E_1)t_3} R_{14}^4 P_{14}^4 e^{-t_3/T_2^D} e^{-t_4/T_2^D} \sum_{i=1}^{i=4} e^{-t_1/T_2^S} \\ &\times M_{ia}^* e^{-t_2/T_2^S} U_{ia} \sum_{j=1}^{j=4} e^{-t_5/T_2^S} V_{ja} e^{-t_6/T_2^S} W_j, \end{aligned} \tag{41}$$

$$\begin{aligned} F_{6b}(t_1,t_2,t_3,t_4,t_5,t_6) &= e^{i\phi^1} e^{-2i\phi^2} e^{-i\phi^3} e^{4i\phi^4} e^{-3i\phi^5} e^{2i\phi^6} e^{-i(E_4-E_1)t_4} \\ &\times e^{-i(E_1-E_4)t_3} R_{41}^4 P_{41}^4 e^{-t_3/T_2^D} e^{-t_4/T_2^D} \sum_{i=1}^{i=4} e^{-t_1/T_2^S} \\ &\times M_{ia}^* e^{-t_2/T_2^S} U_{ib} \sum_{j=1}^{j=4} e^{-t_5/T_2^S} V_{jb} e^{-t_6/T_2^S} W_j, \end{aligned} \tag{42}$$

$$\begin{aligned} F_{6c}(t_1,t_2,t_3,t_4,t_5,t_6) &= e^{-i\phi^1} e^{2i\phi^2} e^{-3i\phi^3} e^{4i\phi^4} e^{-3i\phi^5} e^{2i\phi^6} e^{-i(E_4-E_1)t_4} \\ &\times e^{-i(E_1-E_4)t_3} R_{41}^4 P_{41}^4 e^{-t_3/T_2^D} e^{-t_4/T_2^D} \sum_{i=1}^{i=4} e^{-t_1/T_2^S} \\ &\times M_{ia} e^{-t_2/T_2^S} U_{ic} \sum_{j=1}^{j=4} e^{-t_5/T_2^S} V_{jb} e^{-t_6/T_2^S} W_j, \end{aligned} \tag{43}$$

$$\begin{aligned} F_{6d}(t_1,t_2,t_3,t_4,t_5,t_6) &= e^{-i\phi^1} e^{2i\phi^2} e^{i\phi^3} e^{-4i\phi^4} e^{i\phi^5} e^{2i\phi^6} e^{-i(E_1-E_4)t_4} \\ &\times e^{-i(E_4-E_1)t_3} R_{14}^4 P_{14}^4 e^{-t_3/T_2^D} e^{-t_4/T_2^D} \sum_{i=1}^{i=4} e^{-t_1/T_2^S} \\ &\times M_{ia} e^{-t_2/T_2^S} U_{id} \sum_{j=1}^{j=4} e^{-t_5/T_2^S} V_{ja} e^{-t_6/T_2^S} W_j. \end{aligned} \tag{44}$$

The terms U, V, W are given in Appendix E. M is given in Appendix D while R and P can be calculated using Eqs. (19) and (24), respectively. Finally, the six pulse signal for each orientation, including Gaussian inhomogeneous broadening can be written as

$$F_+^6 = (F_{6a}+F_{6b}+F_{6c}+F_{6d}) e^{-2\pi^2\Delta_G^2(t_5-t_6)^2}. \tag{45}$$

The full powder signal is calculated using Eqs. (45) and (26).

Using Eqs. (45) a number of simulations were carried out for the six pulse sequence. We found two features of relevance: (a) the strength of the powder signal is about 2 orders of magnitude lower than that for the DQM experiment and (b) we find from simulations that the modulation of the powder signal does not directly reflect the strength of the dipolar interaction as compared to the DQM experiment. Signals based on forbidden coherence pathways turn out be stronger than the primary one!

These features are essentially due to the fact that this primary double quantum signal lacks the orientational selectivity (cf. last section) of the DQM experiment. Since the

entire range of dipolar interactions (due to the dependence of the effective dipolar interaction on $3\cos^2\theta-1$) contribute to the signal one obtains a smeared out spectrum. This spread also results in a much reduced amplitude of the DQ spectrum. Therefore, the experimental success of such a refocused echo would require an imposed source of orientational ordering (for example, a bilabeled single crystal or a biradical in a liquid crystal oriented in the magnetic field). Also, improvements in the spectrometer, especially reductions in the instrumental dead times between pulses and better irradiating B_1 fields should enable this experiment. The primary virtue of this experiment would be a measurement of the DQ relaxation rates.

VI. COMPARISON WITH EXPERIMENT

Now we would like to compare our results with the previous experiments. We performed 2D ESR experiments on a bilabeled poly-proline (**P**) peptide system C*PPPPC* spin labeled with a methanethiosulphonate spin label on the cysteines (**C**). For comparison we used a similar peptide monoradical, APPPPC*, where **A** is the peptide alanine. Experimental details are provided elsewhere.[1] However, relevant details are reproduced here. The nominal pulse sequence consisted of a nominal $\pi/2\rightarrow\pi\rightarrow\pi/2\rightarrow\pi\rightarrow\pi/2$ sequence. A true nonselective π pulse (i.e., the second pulse in this sequence) would reverse all coherences, (i.e., $+1\rightarrow-1$ and not provide $+1\rightarrow0$, cf. coherence pathways (i) and (ii) in Sec. IV). Additionally, the third pulse, if it were truly nonselective, would not yield the $0\rightarrow\pm2$ transfer. As noted above, our pulses are not truly nonselective. The estimated irradiating field of the microwave pulses, B_1, is about 18 G, in the rotating frame, whereas the extent of the rigid limit powder nitroxide spectrum is about ±42 G. This results in two kinds of imperfections.[1] (1) The rotation of the spins is not precisely π or $\pi/2$ across the spectrum and (2) the dipolar term can act as a perturbation during the pulse, leading to extra coherences. This was accounted for in our Letter[1] by recognizing that the second pulse is not a perfect π pulse, so it will rotate the spins by an angle different from π, and we added the perturbative contributions due to the dipolar interactions during the third pulse in a simple fashion.[1,35,36] We dealt with these issues more rigorously in this paper, by using SHT[16] as described in Sec. II. The second arbitrary pulse transfers $1\rightarrow0$ and the third converts the latter into DQ coherence [as given by Eqs. (35) and (36) in Sec. IV and Appendix D], in analogy with the discussion of two pulse DQ signals (cf. Sec. III B).

In Fig. 14(a) we show the DQM time domain signal as a stack plot. The spectrum is oriented so that the modulation as a function of t_1 can be seen. This modulation in t_1, which carries the dipolar interaction, is clear. In fact, Saxena and Freed[1] were able to virtually ''read off'' the dipolar interaction from this spectrum.

We now turn to the theoretical analysis of this experiment using Eqs. (26) and (37). In this analysis the key parameters are the strength of the dipolar interaction (D) and the Euler angles required to transform the magnetic tensors

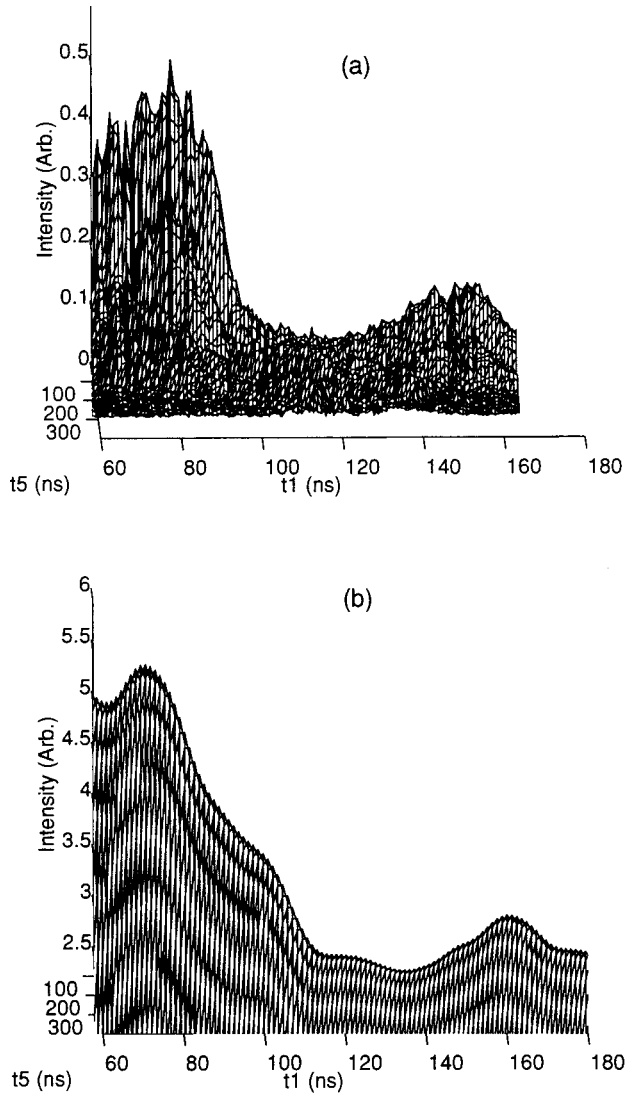

FIG. 14. Experimental DQM spectrum of the biradical peptide and (b) Best fit theoretical simulation. The strength of the irradiation field was 17.8 G. The simulation parameters are: $D=4.4$ G, $\beta_1=180°$, $\beta_2=180°$, $T_2^S=300$ ns, $T_2^D=150$ ns $\Delta_G=2G$. The strength of the irradiation field, B_1, was 17.8 G. The duration of the pulses were: $P_1=P_3=P_5=5$ ns and $P_2=P_4=10$ ns. The other parameters are the same as in Fig. 4. Note that in our earlier Letter we labeled t_1 as t_p.

(g and A) from their PAS to the dipolar frame. The five angles required are shown in Fig. 1. For simplicity, we have chosen to vary only β_1 and β_2 which refer to the angle between the respective nitrogen pi orbitals and the interelectron vector. Therefore, the relative orientation of the nitroxides in this simple picture is related to $|\beta_1-\beta_2|$ (cf. Fig. 1). We used the literature value[41] for the magnetic tensors: $g_{xx}=2.0086$, $g_{yy}=2.0066$, $g_{zz}=2.0032$ and $A_{xx}=A_{yy}=6.23$ and $A_{zz}=35.7$. The other parameters required are the single and double quantum relaxation rates, T_2^S and T_2^D, respectively. These were determined from SECSY (which provides T_2^S) and DQ-COSY (which provides T_2^D: cf. above and Ref. 1) experiments, on the biradical. These parameters are summarized in Tables IV and Tables V. Note that in this analysis we integrate over the angles θ and ζ that describe the orien-

TABLE IV. List of parameters in the simulations.

Parameter	Symbol
Dipolar Interaction	D (G)
Euler angles g frame to dipolar frame for nitroxide 1	$(\alpha_1,^{a}\ \beta_1,\ 0)$
Euler angles g frame to dipolar frame for nitroxide 2	$(\alpha_2,^{a}\ \beta_2,\ \gamma_2^{a})$

[a]These parameters are relatively unimportant and are arbitrarily kept fixed at zero.

tation of the dipolar vector with respect to the dc magnetic field. Hence, we do not make any *ansatz* about the specific values of θ and ζ that our experiment is favoring due to its orientational selectivity.

Figure 14(b) shows the theoretical spectra obtained from our procedure. The relevant parameters obtained are an interelectron distance of 18.5 Å, $\beta_1=180°$, and $\beta_2=180°$.

We note that the fit of Fig. 14(b), while a good one, does not completely capture the details of the experiment. For example, the first maximum in t_1 occurs at a smaller value (and is sharper) in the theory. The second maximum comes at a later t_1 when compared to the experiment. This is probably due to the fact that we have not explored the parameter space exhaustively. For example, we have arbitrarily set $\alpha_1=\alpha_2=\gamma_2=0°$. The inclusion of these would have a small effect on the quality of fit. We believe that an automated procedure for nonlinearly fitting the experiments to theory would result in even better fits and more accurate parameters.[42] Perhaps, more important, we have for simplicity, neglected a distribution in distances. Such a distribution is expected to be present in the sample. In fact, the orientations of the nitroxides themselves would be characterized, more realistically, by a distribution. These distributions would broaden the echo shape in t_1 and should result in fits that are closer to the experiment. Finally, we do not discount the possibility of residual motions at this temperature.

Despite these limitations, we believe that given the nature of the problem, the fit is very encouraging and serves to validate the key hypotheses of our earlier Letter,[1] viz.

(a) The signals are due to forbidden DQ coherences created by arbitrary pulses.
(b) The DQM experiment is an orientationally selective one.

TABLE V. List of fixed parameters in the simulations.

Parameter	Source
g tensors	Literature value
A tensors	Literature value
Homogeneous single quantum linewidth, T_2^{SQ}	SECSY
Homogeneous double quantum linewidth, T_2^{DQ}	DQCOSY

VII. SUMMARY

A theory for calculating rigid limit 2D-DQ ESR spectra for biradicals has been developed. Detailed expressions were provided which include the dipolar interaction and the fully anisotropic g and hf tensors for the nitroxides, as well as the Euler angles required to define the angular geometry of the biradicals. The effect of the strong but not completely nonselective pulses that exist in 2D ESR (and in solid state NMR) was included explicitly by adapting split Hamiltonian theory for numerical simulations. The theory was used to fit DQM experimental spectra obtained from a model polyproline peptide system, (cf. Sec. VI). A distance of 18.5 Å was found which compares well with the value obtained by fluorescence energy transfer measurements.

The DQ 2D ESR technique is shown to provide an attractive method for the measurement of large distances (i.e., $\gtrsim 20$ Å) in bilabeled molecules or between paramagnetic sites in a solid. In this case the dipolar interaction is very weak (about 2 G or less) compared to the dominant g and hf terms, (which provide a spectral extent of about ± 42 G). Using standard phase cycling techniques, the DQ signal due to the dipolar interaction is cleanly obtained, without any interference from the primary, or single quantum signal. Thus any correction for monoradical impurities and/or calibration with a monoradical spectrum is obviated.

However, the complex nature of the spin Hamiltonian in ESR as well as the short relaxation times characteristic of ESR samples provide a significant challenge to obtaining DQ signals using standard techniques (cf. Sec. V). Hence methods that rely on arbitrary pulses for creating DQ coherences are necessitated (cf. Secs. III B and IV). These ''forbidden'' coherences are shown to be highly orientationally selective, thereby providing high resolution ''single-crystal-like'' results from unoriented frozen samples. Hence they are very sensitive to the strength of the dipolar interaction. The product operator technique in conjunction with split Hamiltonian theory is used to qualitatively demonstrate how such ''forbidden'' coherences are created by arbitrary pulses, and why they are orientationally selective. We note that while such ''forbidden'' coherences were obtained in NMR as early as 1958,[35] it is only very recently (1995–) that they have begun to be experimentally exploited in NMR.[14,17,18]

Finally, we would like to point out that these DQ methods also provide a way to measure double quantum relaxation rates, which can be used to elucidate motional dynamics. A key application would be a distinction between global dynamics versus local motions, an area of significant interest for protein dynamics.

ACKNOWLEDGMENTS

We would like to thank Dr. J. Lin and Professor T. Thannhauser for the synthesis of the peptides samples. Program development and computations were performed at the Cornell Theory Center and the Cornell Materials Science Center. This work was supported by NIH Grant No. RR 07126 and NSF Grant No. CHE 9615910.

APPENDIX A: HAMILTONIAN FOR NITROXIDE BIRADICAL

In this Appendix we provide terms C_i, A_i, and B_i used in Eq. (2) in the main text. The Hamiltonian, H_1 and H_2 [cf. Eq. (1)] for this system can be conveniently written as a contraction of irreducible spherical tensor operators (ISTO).[43–45]

$$H_i=\sum_{\mu_i,L,M} F^{L,M}_{\mu_i,l}{}^{*}A^{L,M}_{\mu_i,l}, \quad i=1,2, \tag{A1}$$

where $A^{L,M}_{\mu_i,l}$ contain the spin operators and μ_i refers to the kind of interaction [Zeeman (g) or hyperfine (hf)]. F is proportional to the ISTO of the magnetic interaction (i.e., g and hf). The g and hf tensor (i.e., $F^{L,M}_{\mu_i,l}{}^{*}$) and the relevant spin operators (i.e., $A^{L,M}_{\mu_i,l}$) in irreducible form are given by Schneider and Freed[44] and are reproduced here, for convenience. The irreducible spherical tensor form (ISTO) of the g tensor is[44]

$$\begin{aligned}
&F^{0,0}_{g_i,g_i}=-\sqrt{\frac{1}{3}}\frac{\beta_e}{\hbar}(g_{xx_i}+g_{yy_i}+g_{zz_i}), \quad A^{0,0}_{g_i,l}=-\sqrt{\frac{1}{3}}B_0S_{z_i},\\
&F^{2,0}_{g_i,g_i}=-\sqrt{\frac{2}{3}}\frac{\beta_e}{\hbar}\left[g_{zz_i}-\frac{1}{2}(g_{xx_i}+g_{yy_i})\right],\\
&A^{2,0}_{g_i,l}=-\sqrt{\frac{2}{3}}B_0S_{z_i},\\
&F^{2,\pm1}_{g_i,g_i}=0, \quad A^{2,\pm1}_{g_i,l}=\mp\frac{1}{2}B_0S_{\pm_i},\\
&F^{2,\pm2}_{g_i,g_i}=\frac{1}{2}\frac{\beta_e}{\hbar}(g_{xx_i}-g_{yy_i}), \quad A^{2,\pm2}_{g_i,l}=0.
\end{aligned} \tag{A2}$$

The corresponding components of the hyperfine tensor are

$$\begin{aligned}
&F^{0,0}_{A_i,g_i}=-\sqrt{\frac{1}{3}}\frac{g_e\beta_e}{\hbar}(A_{xx_i}+A_{yy_i}+A_{zz_i}),\\
&A^{0,0}_{A_i,l}=-\sqrt{\frac{1}{3}}\left[S_{z_i}I_{z_i}+\frac{1}{2}(S_{+_i}I_{-_i}+S_{-_i}I_{+_i})\right],\\
&F^{2,0}_{A_i,g_i}=-\sqrt{\frac{2}{3}}\frac{g_e\beta_e}{\hbar}\left[A_{zz_i}-\frac{1}{2}(A_{xx_i}+A_{yy_i})\right],\\
&A^{2,0}_{A_i,l}=-\sqrt{\frac{2}{3}}\left[S_{z_i}I_{z_i}-\frac{1}{4}(S_{+_i}I_{-_i}+S_{-_i}I_{+_i})\right],\\
&F^{2,\pm1}_{A_i,g_i}=0, \quad A^{2,\pm1}_{A_i,l}=\mp\frac{1}{2}\left[S_{\pm_i}I_{z_i}+\frac{1}{4}(S_{z_i}I_{\pm_i})\right],\\
&F^{2,\pm2}_{A_i,g_i}=\frac{1}{2}\frac{g_e\beta_e}{\hbar}(A_{xx_i}-A_{yy_i}), \quad A^{2,\pm2}_{A_i,l}=\frac{1}{2}S_{\pm_i}I_{\pm_i}.
\end{aligned} \tag{A3}$$

Since the F's are most conveniently defined in the molecular axis [i.e., the principle axis system, PAS, of each nitroxide (cf. Fig. 1). Note, that we consider the hf and g tensors of each nitroxide to share the respective PAS, i.e., we assume that there is no tilt between the respective hf and g tensor axis.] we need to transform them to the lab frame. Choosing the dipolar axis as the main symmetry axis of the molecule, we can define this sequence, for the g and hf tensors as (a) a transformation from the respective magnetic frame (g) to the dipolar frame (D) followed by (b) a transformation from the dipolar (D) frame to the laboratory frame (l). This sequence is shown in Fig. 1 and can be written as

$$\begin{aligned}
F^{L,M}_{\mu_i,l}{}^{*}&=\sum_{m',m''}D^{L}_{m,m'}(\Omega_{l\to D})D^{L}_{m',m''}(\Omega_{D\to g_i})F^{L,m''}_{\mu_i,g}\\
&=\sum_{m',m''}D^{L}_{m,m'}(\eta)D^{L}_{m',m''}(\lambda_i)F^{L,m''}_{\mu_i,g},
\end{aligned} \tag{A4}$$

where $\Omega_{D\to g_i}=\lambda_i$ and $\Omega_{l\to D}=\eta$ are the Euler angles defining the transformations from the D to the g_i frame [given by $\lambda_i\equiv(\alpha_i,\beta_i,\gamma_i)$] and from the laboratory frame to the dipolar frame [given by $\eta\equiv(0,\theta,\zeta)$]. Note that if we assume an axially symmetric dipolar tensor (as is reasonable for such long distance biradicals) then the direction of y_d (cf. Fig. 1) can be chosen such that $\gamma_1=0$ (cf. Fig. 1). Given that $F^{2,\pm1}_{\mu_i,g}=0$ and $F^{2,2}_{\mu_i,g}=F^{2,-2}_{\mu_i,g}$ [cf. Eqs. (A2) and (A3)] we can write

$$H_i=\sum_{\mu_i,m}F^{2,m}_{\mu_i,l}{}^{*}A^{2,m}_{\mu_i,l}+\sum_{\mu_i}F^{0,0}_{\mu_i,l}{}^{*}A^{0,0}_{\mu_i,l}. \tag{A5}$$

In high fields and the near rigid limit, the contribution of non secular terms ($S_{\pm_i}$, $S_{\pm_i}I_{z_i}$, $S_{\pm_i}I_{\pm_i}$, $S_{\pm_i}I_{\mp_i}$) is relatively small, and so retaining only the secular and pseudosecular terms we obtain

$$\begin{aligned}
H_i=&\left[\frac{\beta_e}{3\hbar}(g_{xx_i}+g_{yy_i}+g_{zz_i})\right.\\
&\left.+\sqrt{\frac{2}{3}}\sum_{m'}D^{2}_{0,m'}(\eta)K_{g_i,m'}(\lambda_i)\right]B_0S_{z_i}+\left[\frac{g_e\beta_e}{3\hbar}(A_{xx_i}\right.\\
&\left.+A_{yy_i}+A_{zz_i})+\sqrt{\frac{2}{3}}\sum_{m'}D^{2}_{0,m'}(\eta)K_{A_i,m'}(\lambda_i)\right]S_{z_i}I_{z_i}\\
&+\frac{1}{2}\sum_{m'}D^{2}_{-1,m'}(\eta)K_{A_i,m'}(\lambda_i)S_{z_i}I_{-1_i}\\
&-\frac{1}{2}\sum_{m'}D^{2}_{1,m'}(\eta)K_{A_i,m'}(\lambda_i)S_{z_i}I_{+1_i}\\
=&C_iS_{z_i}+A_iS_{z_i}I_{z_i}+B_iS_{z_i}I_{+1_i}+B^{*}S_{z_i}I_{-1_i},
\end{aligned} \tag{A6}$$

where $K_{\mu_i,m'}(\lambda_i)$ contains the transformation from the magnetic to the dipolar frame, and it is defined by

$$K_{\mu_i,m'}(\lambda_i)=[D^2_{m',2}(\lambda_i)+D^2_{m',-2}(\lambda_i)]F^{2,2}_{\mu_i,g}+D^2_{m',0}(\lambda_i)F^{2,0}_{\mu_i,g}. \tag{A7}$$

The terms A_i and C_i are then given by

$$C_i=\sum_{m'} D^2_{0,m'}(\eta_i)K_{g_i,m'}(\lambda_i), \tag{A8}$$

$$A_i=\sum_{m'} D^2_{0,m'}(\eta_i)K_{A_i,m'}(\lambda_i). \tag{A9}$$

The summation in Eqs. (A8) and (A9) can be written explicitly as

$$\begin{aligned}\sum_{m'} D^2_{0,m'}(\eta_i)K_{\mu_i,m'}(\lambda_i)&\equiv\sum_{m'} D^2_{0,m'}(0,\theta,\zeta)K_{\mu_i,m'}(\alpha_i,\beta_i,\gamma_i)\\&=\sqrt{\frac{3}{8}}\sin^2\theta\left[\left\{2\cos^4\frac{\beta_i}{2}\cos 2(\alpha_i+\gamma_i+\zeta)+2\sin^4\frac{\beta_i}{2}\cos 2(\alpha_i-\gamma_i+\zeta)\right\}F^{2,2}_{\mu_i,g_i}\right.\\&\quad\left.+2\sqrt{\frac{3}{8}}\sin^2\beta_i\cos 2(\alpha_i+\zeta)F^{2,0}_{\mu_i,g_i}\right]+\frac{1}{2}(3\cos^2\theta-1)\left[2\sqrt{\frac{3}{8}}\sin^2\beta_i\cos 2\gamma_i F^{2,2}_{\mu_i,g_i}\right.\\&\quad\left.+\frac{1}{2}(3\cos^2\beta_i-1)F^{2,0}_{\mu_i,g_i}\right]+\sqrt{\frac{3}{2}}\sin\theta\cos\theta\sin\beta_i\\&\quad\times\left[\left\{(1+\cos\beta_i)\cos(\alpha_i+2\gamma_i+\zeta)+(\cos\beta_i-1)\cos(2\gamma_i-\alpha_i-\zeta)\right\}F^{2,2}_{\mu_i,g_i}\right.\\&\quad\left.-2\sqrt{\frac{3}{2}}\cos\beta_i\cos(\alpha_i+\zeta)F^{2,0}_{\mu_i,g_i}\right].\end{aligned} \tag{A10}$$

Also B_i is given by

$$\begin{aligned}2B_i&=\sum_{m'} D^2_{1,m'}(\eta_i)K_{A_i,m'}(\lambda_i)\\&\equiv\sum_{m'} D^2_{0,m'}(0,\theta,\zeta)K_{A_i,m'}(\alpha_i,\beta_i,\gamma_i)=\frac{e^{-2i\zeta}}{2}\sin\theta(1+\cos\theta)\left[\left\{\cos^4\frac{\beta_i}{2}e^{-2i(\gamma_i+\alpha_i)}+\sin^4\frac{\beta_i}{2}e^{-2i(\alpha_i-\gamma_i)}\right\}F^{2,2}_{A_i,g_i}\right.\\&\quad\left.+\sqrt{\frac{3}{8}}\sin^2\frac{\beta_i}{2}e^{-2i\alpha_i}F^{2,0}_{A_i,g_i}\right]+\frac{e^{2i\zeta}}{2}\sin\theta(\cos\theta-1)\left[\left\{\sin^4\frac{\beta_i}{2}e^{-2i(\gamma_i-\alpha_i)}+\cos^4\frac{\beta_i}{2}e^{2i(\gamma_i+\alpha_i)}\right\}F^{2,2}_{A_i,g_i}\right.\\&\quad\left.+\sqrt{\frac{3}{8}}\sin^2\frac{\beta_i}{2}e^{2i\alpha_i}F^{2,0}_{A_i,g_i}\right]+\frac{e^{-i\zeta}}{2}(2\cos\theta-1)(1+\cos\theta)\sin\beta_i\left[\frac{1}{2}\{(\cos\beta_i+1)e^{-i(2\gamma_i+\alpha_i)}\right.\\&\quad\left.+(\cos\beta_i-1)e^{-i(\alpha_i-2\gamma_i)}\}F^{2,2}_{A_i,g_i}-\sqrt{\frac{3}{2}}\cos\beta_i e^{-i\alpha_i}F^{2,0}_{A_i,g_i}\right]-\frac{e^{i\zeta}}{2}(2\cos\theta+1)(1-\cos\theta)\\&\quad\times\sin\beta_i\left[\frac{1}{2}\{(\cos\beta_i-1)e^{-i(2\gamma_i-\alpha_i)}+(\cos\beta_i+1)e^{i(\alpha_i+2\gamma_i)}\}F^{2,2}_{A_i,g_i}-\sqrt{\frac{3}{2}}\cos\beta_i e^{i\alpha_i}F^{2,0}_{A_i,g_i}\right]+\frac{1}{2}(3\cos^2\theta-1)\\&\quad\times\left[2\sqrt{\frac{3}{8}}\sin\beta_i\cos 2\gamma_i F^{2,2}_{A_i,g_i}+\frac{1}{2}(3\cos^2\beta_i-1)F^{2,0}_{A_i,g_i}\right].\end{aligned} \tag{A11}$$

The terms C, A, and B [cf. Eqs. (A8), (A9), and (A11)] then contain the anisotropies in the g and hf tensors as well as the Euler angles needed to transform these from their respective principal axis systems to the laboratory frame. Note that C and A are real while B is complex. This completes the definition of H_1 and H_2.

APPENDIX B: MATRIX REPRESENTATION

In this Appendix we provide analytical expressions for the eigenvalues, E_{ij} [that describe the resonant frequency cf. Eq. (15)] of the Hamiltonian, H given in Eq. (1). We also derive the matrix representation of e^{-iHt} required implicitly

for solving the evolution of χ [cf. Eq. (13)] in Eq. (16) and for constructing the pulse propagators R and P [Eqs. (19) and (24)].

We begin by constructing an eigenbasis for the Hamiltonian, H. For a powder an average over all the angular distributions of θ and ζ (cf. Appendix A and Fig. 1) should be taken. For a particular orientation of the biradical the Hamiltonian, H_1, can expressed in matrix form using as a basis set the direct product of the electron spin function ($|+\rangle$ and $|-\rangle$) and the nuclear basis functions $|m_1\rangle$. For ^{14}N, the nuclear basis functions are: $|1\rangle$, $|0\rangle$, and $|-1\rangle$. Hamiltonian H_1 [Eq. (2)] can be written in this basis as:

$$
H_1 = \begin{array}{c}
\begin{array}{cccccc} |+,\mathbf{1}\rangle & |+,\mathbf{0}\rangle & |+,-\mathbf{1}\rangle & |-,\mathbf{1}\rangle & |-\mathbf{1},\mathbf{0}\rangle & |-,-\mathbf{1}\rangle \end{array} \\
\begin{pmatrix}
\frac{C_1}{2}+\frac{A_1}{2} & \frac{B_1}{\sqrt{2}} & 0 & 0 & 0 & 0 \\
\frac{B_1^*}{\sqrt{2}} & \frac{C_1}{2} & \frac{B_1}{\sqrt{2}} & 0 & 0 & 0 \\
0 & \frac{B_1^*}{2} & \frac{C_1}{2}-\frac{A_1}{2} & 0 & 0 & 0 \\
0 & 0 & 0 & -\frac{C_1}{2}-\frac{A_1}{2} & -\frac{B_1}{2} & 0 \\
0 & 0 & 0 & -\frac{B_1^*}{\sqrt{2}} & -\frac{C}{2} & -\frac{B_1}{\sqrt{2}} \\
0 & 0 & 0 & 0 & -\frac{B_1^*}{\sqrt{2}} & -\frac{C_1}{2}+\frac{A_1}{2}
\end{pmatrix}
\end{array}. \tag{B1}
$$

Similar expression for the case of ^{15}N are provided by Lee *et al.*[33] The Hamiltonian, H_1 is diagonalized by the similarity transform $\mathbf{T}^\dagger \mathbf{H_1} \mathbf{T} = \Lambda_1$, where

$$
\mathbf{T} = \begin{pmatrix} \mathbf{T}_\alpha & 0 \\ 0 & \mathbf{T}_\beta \end{pmatrix}. \tag{B2}
$$

H_1 is then diagonal in its eigenbasis composed of the electron spin functions ($|+\rangle$ and $|-\rangle$) and orthonormalized nuclear functions ($\psi_j^{(1)}$, where $j=1,0,-1$) The eigenvectors ψ_j^1 are linear combinations of $|1\rangle$, $|0\rangle$, $|-1\rangle$, i.e., for example,

$$
|\psi_1^{(1)}\rangle = c_1|1\rangle + c_2|0\rangle + c_3|-1\rangle. \tag{B3}
$$

The diagonal form of H_1, i.e., Λ_1 is given by

$$
\Lambda_1 = \begin{pmatrix}
\frac{C_1}{2}+\frac{1}{2}(A_1^2+4|B_1|^2)^{\frac{1}{2}} & 0 & 0 & 0 & 0 & 0 \\
0 & \frac{C_1}{2} & 0 & 0 & 0 & 0 \\
0 & 0 & \frac{C_1}{2}-\frac{1}{2}(A_1^2-4|B_{1_{|^2}})^{\frac{1}{2}} & 0 & 0 & 0 \\
0 & 0 & 0 & -\frac{C_1}{2}-\frac{1}{2}(A_1^2-4|B_1|^2)^{\frac{1}{2}} & 0 & 0 \\
0 & 0 & 0 & 0 & -\frac{C_1}{2} & 0 \\
0 & 0 & 0 & 0 & 0 & -\frac{C_1}{2}+\frac{1}{2}(A_1^2+4|B_1|^2)^{\frac{1}{2}}
\end{pmatrix}. \tag{B4}
$$

Analogous equations can be written for H_2 and $\psi_j^{(2)}$ can be defined, similarly.

We now construct a basis from the electron singlet–triplet function and the nuclear functions ψ_j^i. This is defined as

$$\begin{aligned}
|a\rangle &= T_+ \otimes |\psi_j^{(1)};\psi_k^{(2)}\rangle \equiv |++\rangle \otimes |\psi_j^{(1)};\psi_k^{(2)}\rangle,\\
|b\rangle &= T_0 \otimes |\psi_j^{(1)};\psi_k^{(2)}\rangle\\
&\equiv \frac{1}{\sqrt{2}}\,[|+-\rangle + |-+\rangle] \otimes |\psi_j^{(1)};\psi_k^{(2)}\rangle,\\
|c\rangle &= S \otimes |\psi_j^{(1)};\psi_k^{(2)}\rangle\\
&\equiv \frac{1}{\sqrt{2}}\,[|+-\rangle - |-+\rangle] \otimes |\psi_j^{(1)};\psi_k^{(2)}\rangle,
\end{aligned} \tag{B5}$$

$$|d\rangle = T_- \otimes |\psi_j^{(1)};\psi_k^{(2)}\rangle \equiv |--\rangle \otimes |\psi_j^{(1)};\psi_k^{(2)}\rangle.$$

The full Hamiltonian, H [Eq. (1)] can be shown to be block diagonal in this basis, i.e.,

$$H = \begin{pmatrix} H_{11} & 0 & 0 & 0\\ 0 & H_{22} & H_{23} & 0\\ 0 & H_{32} & H_{33} & 0\\ 0 & 0 & 0 & H_{44} \end{pmatrix}. \tag{B6}$$

Each element in H is a diagonal 9×9 matrix in the nuclear spins functions, $\psi_j^{(i)}$. The various terms can be explicitly written down as

$$\begin{aligned}
H_{11} &\equiv \langle T_+\psi_j^{(1)}\psi_k^{(2)}|H|T_+\psi_{j'}^{(1)}\psi_{k'}^{(2)}\rangle = \left[\frac{1}{2}\,\{C_1+C_2+(A_1^2+4j|B|^2)^{1/2}j+(A_2^2+4k|B|^2)^{1/2}k\}+\frac{D}{6}\,(3\cos^2\theta-1)\right]\delta_{jj'}\delta_{kk'},\\
H_{22} &\equiv \langle T_0\psi_j^{(1)}\psi_k^{(2)}|H|T_0\psi_{j'}^{(1)}\psi_{k'}^{(2)}\rangle = -\frac{D}{3}\,(3\cos^2\theta-1)\,\delta_{jj'}\delta_{kk'},\\
H_{33} &\equiv \langle S\psi_j^{(1)}\psi_k^{(2)}|H|S\psi_{j'}^{(1)}\psi_{k'}^{(2)}\rangle = 2J\,\delta_{jj'}\delta_{kk'},\\
H_{23} &\equiv \langle T_0\psi_j^{(1)}\psi_k^{(2)}|H|S\psi_{j'}^{(1)}\psi_{k'}^{(2)}\rangle = H_{32} \equiv \langle S\psi_j^{(1)}\psi_k^{(2)}|H|T_0\psi_{j'}^{(1)}\psi_{k'}^{(2)}\rangle\\
&\qquad = \left[\frac{1}{2}\,\{C_1-C_2+(A_1^2+4j|B|^2)^{1/2}j-(A_2^2+4k|B|^2)^{1/2}k\}\right]\delta_{jj'}\delta_{kk'},\\
H_{44} &\equiv \langle T_-\psi_j^{(1)}\psi_k^{(2)}|H|T_-\psi_{j'}^{(1)}\psi_{k'}^{(2)}\rangle = \left[\frac{1}{2}\,\{-C_1-C_2-(A_1^2+4j|B|^2)^{1/2}j-(A_2^2+4k|B|^2)^{1/2}k\}+\frac{D}{6}\,(3\cos^2\theta-1)\right]\delta_{jj'}\delta_{kk'},
\end{aligned} \tag{B7}$$

$\mathbf{j}=\mathbf{1},\mathbf{0},-\mathbf{1}$; $\quad \mathbf{k}=\mathbf{1},\mathbf{0},-\mathbf{1}$.

This Hamiltonian, H [cf. Eq. (1)] is diagonalized by the unitary transformation

$$U^\dagger H U = E, \tag{B8}$$

where U is given by

$$U\begin{pmatrix} 1 & 0 & 0 & 0\\ 0 & \cos\Phi & \sin\Phi & 0\\ 0 & -\sin\Phi & \cos\Phi & 0\\ 0 & 0 & 0 & 1 \end{pmatrix}. \tag{B9}$$

In Eq. (B9) Φ is given by

$$\Phi = \frac{1}{2}\tan^{-1}\frac{2H_{23}}{H_{33}-H_{22}}. \tag{B10}$$

The eigenstate of the Hamiltonian, H [cf. Eq. (1)], can then be written as $|a\rangle$, $|\Xi_a\rangle$, $|\Xi_b\rangle$ and $|d\rangle$. $|\Xi_a\rangle$ and $|\Xi_b\rangle$ are defined as

$$|\Xi_a\rangle = (\cos\Phi|T_0\rangle + \sin\Phi|S\rangle) \otimes |\psi_j^{(1)};\psi_k^{(2)}\rangle, \tag{B11}$$

$$|\Xi_b\rangle = (-\sin\Phi|T_0\rangle + \cos\Phi|S\rangle) \otimes |\psi_j^{(1)};\psi_k^{(2)}\rangle,$$

where $|a\rangle$, $|d\rangle$, $|T_0\rangle$, $|S\rangle$, and $\psi_j^{(i)}$ are given by Eq. (B5) and Φ by Eq. (B10). In this basis, E is given by

$$E = \begin{pmatrix} E_1 & 0 & 0 & 0\\ 0 & E_2 & 0 & 0\\ 0 & 0 & E_3 & 0\\ 0 & 0 & 0 & E_4 \end{pmatrix}, \tag{B12}$$

where the elements in Eq. (B12) are given by

$$\begin{aligned}
E_1 &\equiv \langle T_+\psi_j^{(1)}\psi_k^{(2)}|H|T_+\psi_j^{(1)}\psi_k^{(2)}\rangle\\
&= \frac{1}{2}\,\{C_1+C_2+(A_1^2+4j|B|^2)^{1/2}j+(A_2^2+4k|B|^2)^{1/2}k\}\\
&\quad + \frac{D}{6}\,(3\cos^2\theta-1),
\end{aligned}$$

$$E_2 \equiv \langle \Xi_a \psi_j^{(1)} \psi_k^{(2)} | H | \Xi_a \psi_j^{(1)} \psi_k^{(2)} \rangle$$
$$= J - \frac{D}{6}(3\cos^2\theta - 1) - \Bigg[\Bigg\{ J + \frac{D}{6}(3\cos^2\theta - 1) \Bigg\}^2 + \frac{1}{4}\{(C_1 - C_2) + (A_1^2 + 4j|B|^2)^{1/2} j - (A_2^2 + 4k|B|^2)^{1/2} k\}^2 \Bigg]^{1/2},$$

$$E_3 \equiv \langle \Xi_b \psi_j^{(1)} \psi_k^{(2)} | H | \Xi_b \psi_j^{(1)} \psi_k^{(2)} \rangle$$
$$= J - \frac{D}{6}(3\cos^2\theta - 1) + \Bigg[\Bigg\{ J + \frac{D}{6}(3\cos^2\theta - 1) \Bigg\}^2 + \frac{1}{4}\{(C_1 - C_2) + (A_1^2 + 4j|B|^2)^{1/2} j - (A_2^2 + 4k|B|^2)^{1/2} k\}^2 \Bigg]^{1/2}, \quad \text{(B13)}$$

$$E_4 \equiv \langle T_- \psi_j^{(1)} \psi_k^{(2)} | H | T_- \psi_j^{(1)} \psi_k^{(2)} \rangle = \tfrac{1}{2}(-C_1 - C_2 - (A_1^2 + 4j|B|^2)^{1/2} j - (A_2^2 4k|B|^2)^{1/2} k + \tfrac{1}{6} D(3\cos^2\theta - 1),$$

$$\mathbf{j} = \mathbf{1}, \mathbf{0} - \mathbf{1}; \quad \mathbf{k} = \mathbf{1}, \mathbf{0}, -\mathbf{1}.$$

Note that Eq. (B13) provides the 36 diagonal in elements of E. For compactness of notation we have suppressed multiplication of each term in this equation by $\delta_{jj'}\delta_{kk'}$.

The exponential operator e^{-iHt} can then be expressed as

$$X(t) \equiv e^{-iHt} = U^\dagger e^{-iEt} U. \quad \text{(B14)}$$

Substituting Eqs. (B9), (B12), and (B13) in Eq. (B14) we get

$$e^{-iHt} = \begin{pmatrix} e^{-iE_1 t} & 0 & 0 & 0 \\ 0 & \cos^2\Phi e^{-iE_2 t} + \sin^2\Phi e^{-iE_3 t} & \cos\phi \sin\phi (e^{-iE_2 t} - e^{-iE_3 t}) & 0 \\ 0 & \cos\phi \sin\phi (e^{-iE_2 t} - e^{-iE_3 t}) & \sin^2\Phi e^{-iE_2 t} + \cos^2\Phi e^{-iE_3 t} & 0 \\ 0 & 0 & 0 & e^{-iE_4 t} \end{pmatrix}. \quad \text{(B15)}$$

APPENDIX C: PULSE PROPAGATOR

In this section the exponential operator, $e^{-i\epsilon t_p}$ is derived, in the basis vectors given in (a) Eq. (B5), i.e., the singlet–triplet basis and (b) Eqs. (B11) and (B5), i.e., the eigenbasis.

Expanding the operator, $e^{-i\epsilon t_p}$ in a Taylor series we get

$$e^{-i\epsilon t_p} = \sum_{n=0}^{\infty} \frac{(-i\epsilon t_p)^n}{n!}. \quad \text{(C1)}$$

In the singlet–triplet basis [cf. Eq. (B5)] and using Eq. (9) we find that the odd and even term in the right-hand side of Eq. (C1) obey the recursion relationships given by

$$\epsilon^{2n-1} = \omega_1^{2n-1} A, \quad n = 1,2,\ldots\infty, \quad \text{(C2)}$$

$$\epsilon^{2n} = \omega_1^{2n} A^2, \quad n = 1,2,\ldots\infty, \quad \text{(C3)}$$

where A and A^2 are matrices, that in the singlet–triplet basis of Eq. (B5) are given by

$$A = \begin{pmatrix} 0 & \frac{1}{\sqrt{2}} e^{-i\phi} & 0 & 0 \\ \frac{1}{\sqrt{2}} e^{i\phi} & 0 & 0 & \frac{1}{\sqrt{2}} e^{-i\phi} \\ 0 & 0 & 0 & 0 \\ 0 & \frac{1}{\sqrt{2}} e^{i\phi} & 0 & 0 \end{pmatrix} \quad \text{(C4)}$$

and

$$A^2 = \begin{pmatrix} 1 & 0 & 0 & e^{-2i\phi} \\ 0 & 2 & 0 & 0 \\ 0 & 0 & 0 & 0 \\ e^{2i\phi} & 0 & 0 & 1 \end{pmatrix}. \quad \text{(C5)}$$

In Eqs. (C4) and (C5), ϕ refers to the phase of the pulse [cf. Eq. (9)] and note that $\omega_1 t_p = \beta$ [Eq. (11)]. Also each element in A and A^2 is a 9×9 diagonal matrix in the nuclear spin basis, ψ_j^i. Substituting Eq. (C3) in Eq. (C1) we obtain

$$e^{-i\epsilon t_p} = 1 + iA \sin\beta + A^2(\cos\beta - 1). \quad \text{(C6)}$$

On substituting Eqs. (C4) and (C5) in Eq. (C6) we find that $e^{-i\epsilon t}$, in the singlet–triplet (case a above) representation is:

$$e^{-i\epsilon t_p}=\begin{pmatrix} \frac{1}{2}(\cos\beta+1) & -\frac{i}{\sqrt{2}}\sin\beta e^{-i\phi} & 0 & \frac{1}{2}(\cos\beta-1)e^{-2i\phi} \\ -\frac{i}{\sqrt{2}}\sin\beta e^{i\phi} & \cos\beta & 0 & -\frac{i}{\sqrt{2}}\sin\beta e^{-i\phi} \\ 0 & 0 & 1 & 0 \\ \frac{1}{2}(\cos\beta-1)e^{2i\phi} & -\frac{i}{\sqrt{2}}\sin\beta e^{i\phi} & 0 & \frac{1}{2}(\cos\beta+1) \end{pmatrix}. \tag{C7}$$

Using a similar procedure, we obtain $e^{-i\epsilon t}$ in the eigenbasis of the Hamiltonian, H, (i.e., for case b) given by Eq. (B11) and (B5). This is given by

$$e^{-i\epsilon t}=\begin{pmatrix} (\frac{1}{2}\cos\beta+1) & -\frac{i}{\sqrt{2}}\cos\Phi\sin\beta e^{-i\phi} & \frac{i}{\sqrt{2}}\sin\Phi\sin\beta e^{-i\phi} & \frac{1}{2}(\cos\beta-1)e^{-2i\phi} \\ -\frac{i}{\sqrt{2}}\cos\Phi\sin\beta e^{i\phi} & 1+\cos^2\Phi(\cos\beta-1) & -\cos\Phi\sin\Phi(\cos\beta-1) & -\frac{1}{\sqrt{2}}\cos\Phi\sin\beta e^{-i\phi} \\ \frac{i}{\sqrt{2}}\sin\Phi\sin\beta e^{i\phi} & -\cos\Phi\sin\Phi(\cos\beta-1) & 1+\sin^2\Phi(\cos\beta-1) & \frac{i}{\sqrt{2}}\sin\Phi\sin\beta e^{-i\phi} \\ \frac{1}{2}(\cos\beta-1)e^{2i\phi} & -\frac{i}{\sqrt{2}}\cos\Phi\sin\beta e^{i\phi} & \frac{i}{\sqrt{2}}\sin\Phi\sin\beta e^{i\phi} & \frac{1}{2}(\cos\beta+1) \end{pmatrix}. \tag{C8}$$

Again, each element in Eqs. (C7) and (C8) is a 9×9 diagonal matrix in the nuclear functions, as noted above.

Using Eqs. (B15) and (C7) and we can calculate R and P in Eqs. (19) and (24) to any order in the Trotter exponent, n.

APPENDIX D: FIVE PULSE SIGNAL

In this Appendix we provide the terms M, N, and Q that define the signal observed in the five pulse DQM and DQ-COSY experiments. The terms X, R, P, and S are defined by Eqs. (B14), (19), (24), and Table I, respectively.

$$\begin{aligned}
M_{1a}&=M_{1b}=S_1^1(R_{11}^1P_{12}^1-R_{14}^1P_{42}^1)\\
&\quad+S_2^1(R_{11}^1P_{13}^1-R_{14}^1P_{43}^1),\\
N_{1a}&=R_{41}^3R_{11}^2P_{21}^2P_{11}^3+R_{21}^2P_{22}^2(R_{42}^3X_{22}(t_2)X_{22}^\dagger(t_2)P_{21}^3\\
&\quad+R_{43}^3X_{23}(t_2)X_{32}^\dagger(t_2)P_{31}^3)+R_{44}^3R_{41}^2P_{24}^2P_{41}^3\\
&\quad+R_{31}^2P_{23}^2(R_{43}^3X_{33}(t_2)X_{33}^\dagger(t_2)P_{31}^3\\
&\quad+R_{42}^3X_{32}(t_2)X_{23}^\dagger(t_2)P_{21}^3),\\
M_{2a}&=M_{2b}=S_1^1(R_{11}^1P_{13}^1-R_{14}^1P_{43}^1)\\
&\quad+S_2^1(R_{11}^1P_{12}^1-R_{14}^1P_{42}^1),\\
N_{2a}&=R_{41}^3R_{11}^2P_{31}^2P_{11}^3+R_{21}^2P_{32}^2(R_{42}^3X_{22}(t_2)X_{22}^\dagger(t_2)P_{21}^3\\
&\quad+R_{43}^3X_{23}(t_2)X_{32}^\dagger(t_2)P_{31}^3)+R_{44}^3R_{41}^2P_{34}^2P_{41}^3\\
&\quad+R_{31}^2P_{33}^2(R_{43}^3X_{33}(t_2)X_{33}^\dagger(t_2)P_{31}^3\\
&\quad+R_{42}^3X_{32}(t_2)X_{23}^\dagger(t_2)P_{21}^3),
\end{aligned}\tag{D1}$$

$$\begin{aligned}
M_{3a}&=M_{3b}=S_3^1(R_{31}^1P_{14}^1-R_{34}^1P_{44}^1)\\
&\quad+S_4^1(R_{21}^1P_{14}^1-R_{24}^1P_{44}^1),\\
N_{3a}&=R_{41}^3R_{13}^2P_{41}^2P_{11}^3+R_{23}^2P_{42}^2(R_{42}^2X_{22}(t_2)X_{22}^\dagger(t_2)P_{21}^3\\
&\quad+R_{43}^3X_{23}(t_2)X_{32}^\dagger(t_2)P_{31}^3)+R_{44}^3R_{43}^2P_{44}^2P_{41}^3\\
&\quad+R_{33}^2P_{43}^2(R_{43}^3X_{33}(t_2)X_{33}^\dagger(t_2)P_{31}^3\\
&\quad+R_{42}^3X_{32}(t_2)X_{23}^\dagger(t_2)P_{21}^3),\\
M_{4a}&=M_{4b}=S_3^1(R_{21}^1P_{14}^1-R_{24}^1P_{44}^1)+S_4^1(R_{31}^1P_{41}^1-R_{34}^1P_{44}^1),\\
N_{4a}&=R_{41}^3R_{12}^2P_{41}^2P_{11}^3+R_{22}^2P_{42}^2(R_{42}^3X_{22}(t_2)X_{22}^\dagger(t_2)P_{21}^3\\
&\quad+R_{43}^3X_{23}(t_2)X_{32}^\dagger(t_2)P_{31}^3)+R_{44}^3R_{42}^2P_{44}^2P_{41}^3\\
&\quad+R_{32}^2P_{43}^2(R_{43}^3X_{33}(t_2)X_{33}^\dagger(t_2)P_{31}^3\\
&\quad+R_{42}^3X_{32}(t_2)X_{23}^\dagger(t_2)P_{21}^3),\\
N_{1b}&=R_{11}^1R_{11}^2P_{21}^2P_{14}^3+R_{21}^2P_{22}^2(R_{12}^3X_{22}(t_2)X_{22}^\dagger(t_2)P_{24}^3\\
&\quad+R_{13}^3X_{23}(t_2)X_{32}^\dagger(t_2)P_{34}^3)+R_{14}^3R_{41}^2P_{24}^2P_{44}^3\\
&\quad+R_{31}^2P_{23}^2(R_{13}^3X_{33}(t_2)X_{33}^\dagger(t_2)P_{34}^3\\
&\quad+R_{12}^3X_{32}(t_2)X_{23}^\dagger(t_2)P_{24}^3),\\
N_{2b}&=R_{11}^1R_{11}^2P_{31}^2P_{14}^3+R_{21}^2P_{32}^2(R_{12}^3X_{22}(t_2)X_{22}^\dagger(t_2)P_{24}^3\\
&\quad+R_{13}^3X_{23}(t_2)X_{32}^\dagger(t_2)P_{34}^3)+R_{14}^3R_{41}^2P_{34}^2P_{44}^3\\
&\quad+R_{31}^2P_{33}^2(R_{13}^3X_{33}(t_2)X_{33}^\dagger(t_2)P_{34}^3\\
&\quad+R_{12}^3X_{32}(t_2)X_{23}^\dagger(t_2)P_{24}^3),
\end{aligned}\tag{D2}$$

$$N_{3b}=R^3_{11}R^2_{13}P^2_{41}P^3_{14}+R^2_{23}P^2_{42}(R^3_{12}X_{22}(t_2)X^{\dagger}_{22}(t_2)P^3_{24}$$
$$+R^3_{13}X_{23}(t_2)X^{\dagger}_{32}(t_2)P^3_{34})+R^3_{14}R^2_{43}P^2_{44}P^3_{44}$$
$$+R^2_{33}P^2_{43}(R^3_{13}X_{33}(t_2)X^{\dagger}_{33}(t_2)P^3_{34}$$
$$+R^3_{12}X_{32}(t_2)X^{\dagger}_{23}(t_2)P^3_{24}),$$
$$N_{4b}=R^3_{11}R^2_{12}P^2_{41}P^3_{14}+R^2_{22}P^2_{42}(R^3_{12}X_{22}(t_2)X^{\dagger}_{22}(t_2)P^3_{24}$$
$$+R^3_{13}X_{23}(t_2)X^{\dagger}_{32}(t_2)P^3_{34})+R^3_{14}R^2_{12}P^2_{44}P^3_{44}$$
$$+R^2_{32}P^2_{43}(R^3_{13}X_{33}(t_2)X^{\dagger}_{33}(t_2)P^3_{34}$$
$$+R^3_{12}X_{32}(t_2)X^{\dagger}_{23}(t_2)P^3_{24}),$$

$$Q_{1a}=R^5_{21}P^5_{41}S^{5*}_1,\quad Q_{2a}=R^5_{31}P^5_{41}S^{5*}_2,$$
$$Q_{3a}=R^5_{41}P^5_{42}S^{5*}_3,\quad Q_{4a}=R^5_{41}P^5_{43}S^{5*}_4, \tag{D3}$$

$$Q_{1b}=R^5_{24}P^5_{11}S^{5*}_1,\quad Q_{2b}=R^5_{34}P^5_{11}S^{5*}_2,$$
$$Q_{3b}=R^5_{44}P^5_{12}S^{5*}_3,\quad Q_{4b}=R^5_{44}P^5_{13}S^{5*}_4. \tag{D4}$$

APPENDIX E: SIX PULSE SIGNAL

In this Appendix we provide the terms U, V, and W required to describe the six pulse primary refocussed double quantum echo

$$U_{1a}=S^2_1(R^3_{41}P^3_{21}R^2_{12}P^2_{12})+S^2_2(R^3_{41}P^3_{31}R^2_{12}P^2_{12}),$$
$$U_{2a}=S^2_5(R^3_{41}P^3_{31}R^2_{13}P^2_{13})+S^2_2(R^3_{41}P^3_{21}R^2_{13}P^2_{13}),$$
$$U_{3a}=S^2_6(R^3_{43}P^3_{41}R^2_{34}P^2_{34})+S^2_4(R^3_{42}P^3_{41}R^2_{34}P^2_{34}),$$
$$U_{4a}=S^2_3(R^3_{42}P^3_{41}R^2_{24}P^2_{24})+S^2_4(R^3_{43}P^3_{41}R^2_{24}P^2_{24}), \tag{E1}$$
$$V_{1a}=S^5_1R^5_{11}P^5_{42}+S^5_2R^5_{11}P^5_{43},\quad W_1=S^{6*}_1R^6_{21}P^6_{21},$$
$$V_{2a}=S^5_5R^5_{11}P^5_{43}+S^5_2R^5_{11}P^5_{42},\quad W_2=S^{6*}_2R^6_{31}P^6_{31},$$
$$V_{3a}=S^5_3R^5_{21}P^5_{44}+S^5_4R^5_{31}P^5_{44},\quad W_3=S^{6*}_3R^6_{42}P^6_{42}, \tag{E2}$$
$$V_{4a}=S^5_6R^5_{31}P^5_{44}+S^5_3R^5_{21}P^5_{44},\quad W_4=S^{6*}_4R^6_{43}P^6_{43}.$$

U_{ib} can be obtained from U_{ia} $(i=1,\ 4)$ by making the following substitutions:

$$R^3_{11}P^3_{24}\rightarrow R^3_{41}P^3_{21},\quad R^3_{11}P^3_{34}\rightarrow R^3_{41}P^3_{31},$$
$$R^3_{12}P^3_{44}\rightarrow R^3_{42}P^3_{41},\quad R^3_{13}P^3_{44}\rightarrow R^3_{43}P^3_{41}. \tag{E3}$$

Also V_{ib} is obtained from V_{ia} by the following substitutions:

$$R^5_{14}P^5_{12}\rightarrow R^5_{11}P^5_{42},\quad R^5_{14}P^5_{13}\rightarrow R^5_{11}P^5_{43},$$
$$R^5_{24}P^5_{14}\rightarrow R^5_{21}P^5_{44},\quad R^5_{34}P^5_{14}\rightarrow R^5_{31}P^5_{44}. \tag{E4}$$

Furthermore,

$$U_{ic}=U^*_{ia},\quad U_{id}=U^*_{ib},\quad i=1,4. \tag{E5}$$

[1] S. Saxena and J. H. Freed, Chem. Phys. Lett. **251**, 102 (1996).
[2] S. A. Dzuba, M. K. Bosch, and A. Hoff, Chem. Phys. Lett. **248**, 427 (1996).
[3] M. Forbes and K. Bhagat, J. Am. Chem. Soc. **115**, 3382 (1993).
[4] A. H. Beth, B. H. Robinson, C. E. Cobb, L. R. Dalton, W. E. Trommer, J. J. Birktoft, and J. H. Park, J. Biol. Chem. **259**, 9717 (1984).
[5] G. R. Eaton and S. S. Eaton, in *Biological Magnetic Resonance*, Vol. 8, edited by L. J. Berliner and J. Reuben (Plenum, New York, 1989).
[6] J. Gorcester, G. L. Millhauser, and J. H. Freed, in *Modern Pulsed and Continuous Wave Electron Spin Resonance*, edited by L. Kevan and M. K. Bowman (Wiley, New York, 1990).
[7] J. H. Freed, in *Multiple Electron Resonance Spectroscopy*, edited by M. Dorio and J. H. Freed (Plenum, New York, 1979).
[8] A. D. Milov, A. B. Ponomasev, and Yu. D. Tsvetkov, Chem. Phys. Lett. **110**, 67 (1984).
[9] R. G. Larsen and D. J. Singel, J. Chem. Phys. **98**, 5134 (1993).
[10] V. V. Khurshev, A. M. Raitsimring, and Yu. D. Tsvetkov, J. Magn. Reson. **81**, 441 (1989).
[11] A. Raitsimring, J. Peisach, H. C. Lee, and X. Chen. J. Phys. Chem. **96**, 3526 (1992).
[12] R. Fairclough and C. R. Cantor, Meth. Enzymol. **48**, 347 (1977).
[13] (a) V. S. S. Sastry, A. Polimeno, R. H. Crepeau, and J. H. Freed, J. Chem. Phys. **105**, 5753 (1996); (b) **105**, 5773 (1996); (c) J. Gorcester, S. B. Rananavare, and J. H. Freed, *ibid*. **90**, 5764 (1989); (d) G. L. Millhauser and J. H. Freed, *ibid*. **85**, 63 (1986).
[14] G. Wu, D. Rovnyank, B. Sun, and R. B. Griffin, Chem. Phys. Lett. **249**, 210 (1996).
[15] (a) E. C. Hoffman, G. Jeschke, and A. Schweiger, Chem. Phys. Lett. **248**, 393 (1996); (b) C. Gemperle, A. Schweiger, and R. R. Ernst, J. Magn. Reson. **91**, 273 (1991); (c) G. Jeschke and A. Schweiger, Mol. Phys. **88**, 355 (1996); (d) G. Jeschke and A. Schweiger, J. Chem. Phys. **72**, 2199 (1996).
[16] K. Salikhov, D. J. Schneider, S. Saxena, and J. H. Freed, Chem. Phys. Lett. **262**, 17 (1996).
[17] C. Fernandez and J. P. Amoureux, Chem. Phys. Lett. **242**, 449 (1995).
[18] (a) A. Medek, J. S. Hardwood, and L. Frydman J. Am. Chem. Soc. **117**, 12779 (1995); (b) J. P. Amoureux, C. Fernandez, and L. Frydman, Chem. Phys. Lett. **259**, 327 (1996).
[19] A. Carrington and A. D. McLachlan, *Introduction to Magnetic Resonance with Application to Chemistry and Chemical Physics* (Harper and Row, New York, 1967).
[20] J. Tang and J. R. Norris, Chem. Phys. Lett. **233**, 192 (1995).
[21] D. J. Schneider and J. H. Freed, *Advances in Chemical Physics*, Vol. LXIII, edited by J. O. Hirschfelder, R. E. Wyatt, and R. D. Coalson (Wiley, New York, 1989).
[22] R. R. Ernst, G. Bodenhausen, and A. Wokaun, *Principles of NMR in One and Two Dimension* (Clarendon, Oxford, 1987).
[23] J. H. Freed, G. V. Bruno, and C. F. Polnaszek, J. Phys. Chem. **75**, 3385 (1971).
[24] D. Gamliel and J. H. Freed, J. Magn. Reson. **89**, 60 (1990).
[25] (a) J. Gorcester and J. H. Freed, J. Chem. Phys. **85**, 5375 (1986); (b) J. Gorcester and J. H. Freed, *ibid*. **88**, 4678 (1988).
[26] (a) G. Bodenhausen, R. L. Vold, and R. R. Vold, J. Magn. Reson. **37**, 93 (1980); (b) G. Bodenhausen, R. Freeman, R. Niedermeyer, and D. L. Turner, J. Magn. Reson. **26**, 133 (1977); (c) G. Bodenhausen, R. Freeman, and D. L. Turner, *ibid*. **27**, 511 (1977).
[27] A. Wokaun and R. R. Ernst, J. Chem. Phys. **67**, 1752 (1977).
[28] S. Vega, J. Chem. Phys. **68**, 5518 (1978).
[29] N. C. Nielsen, H. Bildson, and H. J. Jacobsen, Chem. Phys. Lett. **191**, 205 (1992).
[30] M. Suzuki, J. Math. Phys. **26**, 601 (1985).
[31] H. F. Trotter, Proc. Am. Math. Soc. **10**, 545 (1959).
[32] S. Lee, D. E. Budil, and J. H. Freed, J. Chem. Phys. **101**, 5529 (1994).
[33] S. Lee, B. R. Patyal, and J. H. Freed, J. Chem. Phys. **98**, 3665 (1993). This reference distinguishes the terms which are refocused from those which are not in 2D-FT-ESR experiment.
[34] S. Lee, B. R. Patyal, S. Saxena, R. H. Crepeau, and J. H. Freed, Chem. Phys. Lett. **221**, 397 (1994).
[35] I. Solomon, Phys. Rev. **110**, 61 (1958).
[36] A. Abragam, *The Principles of Nuclear Magnetism* (Oxford University Press, New York, 1961), p. 245.
[37] In Eq. (33) we follow the standard approach of Ref. 22 for simplicity. More rigorously, one must carefully distinguish whether the source(s) of inhomogeneous broadening affect the two single quantum coherences dif-

ferently from each other, so their combined effect in the double quantum coherence is not fully canceled by the condition $2t_1=t_2$.
[38] G. Drobny, A. Pines, S. Sinton, D. Weitekamp, and D. Wemmer, Faraday Symp. Chem. Soc. **13**, 49 (1979).
[39] L. J. Schwartz, E. Meirovitch, J. A. Ripmeester, and J. H. Freed, J. Phys. Chem. **87**, 4453 (1983).
[40] C. P. Slichter, *Principles of Magnetic Resonance*, 3rd ed. (Springer, New York, 1990).
[41] S. M. Miick and G. L. Millhauser, Biophys. J. **63**, 917 (1992).
[42] D. E. Budil, S. Lee, S. Saxena, and J. H. Freed, J. Magn. Reson. Ser. A **120**, 155 (1996).
[43] D. M. Brink and G. R. Satchler, *Angular Momentum in Quantum Mechanics*, Vol. 3 (Clarendon, Oxford, 1993).
[44] D. J. Schneider and J. H. Freed, in *Spin Labeling: Theory and Application*, edited by L. J. Berliner and J. Reuben (Plenum, New York, 1989).
[45] P. L. Nordio, *General Magnetic Resonance Theory, in Spin Labeling: Theory and Applications*, Vol. 1, edited by L. J. Berliner (Academic, New York, 1976), Chap. 2.